MODELING AND CLUSTERING ANALYSIS OF PULMONARY CRACKLES

by

Mete YEĞİNER

B.S., in Physics, Bogazici University, 1999

M.S., in Biomedical Science, Bogazici University, 2002

Submitted to the Institute of Biomedical Engineering

in partial fulfillment of the requirements

for the degree of

Doctor

of

Philosophy

Boğaziçi University

June 2008

MODELING AND CLUSTERING ANALYSIS OF PULMONARY CRACKLES

APPROVED BY:

Assoc.Prof. Yasemin P. Kahya .....
(Thesis Advisor)

Prof. Ayşın B. Ertüzün .....

Prof. Ahmet Ademoğlu .....

Prof. Yekta Ülgen .....

Prof. Günseli Kılınç .....

DATE OF APPROVAL: June 16, 2008

ACKNOWLEDGMENTS

I, firstly, appreciate Prof. Yasemin P. Kahya for playing key role in both going over obstacles during my dissertation process and opening new windows (not Microsoft's) to the light of the unique solutions. Inspiring from the words of F. Bloch who is one of PhD students of W. Heisenberg, I can say that I have watched "'the spirit of research" through the opened windows.

Secondly, thanks to the members of our laboratory, i.e. Koray Çiftçi and Ipek Şen for their supports while we all simultaneously face with the similar problems during our studies and experiments.

I appreciate Prof. Ahmet Ademoğlu, Prof. Ayşın B. Ertüzün and Prof. Yekta Ülgen for completing the deficiencies of my studies by their worthy advices.

I thank Prof. Gunseli Kilinc, MD, from Istanbul University Cerrahpasa Medical School and Sibel Yurt, MD, from Yedikule Teaching Hospital for Chest Diseases and Thoracic Surgery for their guidance and advices on data acquisition and diagnosis of pulmonary disorders of patients.

At the end, it is beyond the domain of the words to thank the supports and the contributions of my family in the all stages of my life.

ABSTRACT

MODELING AND CLUSTERING ANALYSIS OF PULMONARY CRACKLES

The objective of this study is to perform two complementary analyses of pulmonary crackles, i.e. modeling and clustering, in order to interpret crackles in time-frequency domain and also determine the optimal number of crackle types and their characteristics using the modeling parameters. Since the crackles are superimposed on background vesicular sounds, a preprocessing method for the elimination of vesicular sounds from crackle waveform is also proposed for achieving accurate parameterization. The proposed modeling method, i.e. the wavelet network modeling, interprets the transient structure of crackles in the time-frequency space with a small number of components using the time-localization property of wavelets. In modeling analysis, complex Morlet wavelets are selected as transfer functions in the hidden nodes due to both their similarity with the crackle waveforms and their flexibility in the modeling process. Clustering analysis of crackles probe the discrepancies found among the studies related with the crackle types and their corresponding characteristics. Since, in these studies, crackles are classified according to the auditory perception of the observers, there are inconsistencies found in the labeling of the same crackle. To overcome the inherent subjectivity, the crackles are classified in an unsupervised method using the EM clustering analysis. In this method, it is assumed that the crackle data can be interpreted with the multivariate Gaussian mixture model and, therefore, crackle clusters distribute normally in the feature spaces. The results strongly suggest the existence of a third crackle type, medium, in addition to the commonly used two types, i.e. fine and coarse. Moreover, the extracted characteristics of crackle types offer additional features for the computerized crackle-based analysis of pulmonary disorders.

Keywords: Lung Sounds, Pulmonary Crackles, Crackle Types, Wavelet Networks, Signal Modeling, EM Clustering, Vesicular Sound Elimination

ÖZET

SOLUNUM SESİ ÇITIRTILARININ MODELLENMESİ VE ÖBEKLEME ANALİZİ

Bu çalışmanın hedefi, solunum çıtırtılarının birbirini tamamlayan iki analizi olan modelleme ve öbeklemeyi gerçekleştirerek çıtırtıları zaman-sıklık uzayında ifade etmek ve çıtırtı türlerinin en uygun sayısını ve özelliklerini belirlemektir. Çıtırtıların ardalandaki vesikular sesin üzerine eklenmesi nedeniyle, parametreleme analizini doğru yapabilmek için, çıtırtı sinyalinden vesikular sesin temizlenmesi amacıyla bir ön-işlem yöntemi de önerilmiştir. Önerilen modelleme yöntemi olan dalgacık ağları ile modelleme, dalgacık enerjisinin zaman uzayındaki derişiminden faydalanarak daha az bileşen ile çıtırtının geçici yapısını zaman-sıklık uzayında ifade etmektedir. Modelleme analizinde, kompleks Morlet dalgacıkları, hem Morlet dalgacığı ile çıtırtının dalga şekillerinin benzerliğinden hem de modellemedeki esnek performansından dolayı saklı düğümlerde transfer fonksiyonu olarak kulanılmıştır. Öbekleme analizi çıtırtıların tür sayıları ve bunların özellikleri hakkında yapılan çalışmaların tutarsızlığı nedeni ile yapılmıştır. Bu çalışmalarda çıtırtılar gözlemcilerin duysal algılamalarına göre sınıflandırıldığından, aynı çıtırtıyı etiketlemede farlılıklar ortaya çıkmaktadır. Bu öznelliğin üstesinden gelebilmek için, çıtırtılar EM öbekleme analiziyle yönlendirmesiz olarak sınıflandırılmıştır. Bu yöntemde çıtırtı verisinin çok-değişkenli Gauss karışım modeli olarak ifade edilebileceği ve böylece çıtırtı öbeklerinin bileşen uzaylarında normal bir dağılım göstereceği öngörülmüştür. Sonuçlar genellikle kullanılan iki tür olan ince ve kalın çıtırtıların yanında üçüncü bir tür olan orta çıtırtının varlığı konusunda güçlü deliller sunmaktadır. Buna ek olarak, çıtırtı türlerinin nitelendirilmesi, solunum rahatsızlıklarının çıtırtı tabanlı bilgisayar analizine yeni öğeler önermiştir.

Anahtar Sözcükler: Solunum Sesleri, Solunum Çıtırtıları, Çıtırtıların Türleri, Dalgacık Ağları, Sinyal Modelleme, EM Öbekleme, Vesikular Sesin Temizlenmesi

TABLE OF CONTENTS

LIST OF FIGURES

LIST OF TABLES

LIST OF SYMBOLS

a_k	Scaling parameter of k^{th} node of WN
b_k	Time-shifting parameter of k^{th} node of WN
f_c	Cut-off Frequency
f_c^{est}	Estimated Cut-off Frequency
f_c^{fit}	Fitted Cut-off Frequency
f_c^{opt}	Optimum Cut-off Frequency
$w_{cos,k}$	Weight factor of cosine term of WN
$w_{sin,k}$	Weight factor of sine term of WN
ω_k	Modulating frequency of k^{th} node of WN

LIST OF ABBREVIATIONS

$2CD$	Two-Cycle Duration
AER	Absolute Error Rate
$mAER$	Mean of Absolute Error Rates
AIC	Akaike Information Criterion
ATS	American Thoracic Society
BIC	Bayesian Inference Criterion
CC	Coarse Crackle
CF	Central Frequency
$COPD$	Chronic Obstructive Pulmonary Disease
$CORSA$	Computerized Respiratory Sound Analysis Research Group
CW	Crackle Window
DT	Distortion Threshold
EM	Expectation-Maximization
ER	Error Rate
FC	Fine Crackle
IDW	Initial Deflection Width
LDW_i	i^{th} Largest Deflection Width
MLP	Multi-layer Perceptron
cM	Complex Morlet
PSD	Power Spectral Density
cPS	Cumulative Power Spectrum
$cPS_{\%}$	Percentile frequencies of cPS
ROI	Region of Interest
VS	Vesicular Sound
WF	Wavelet Filtering
WN	Wavelet Network

1. INTRODUCTION

Auscultation of pulmonary sounds with a stethoscope is a common, inexpensive and noninvasive method in the diagnosis of respiratory disorders. However due to the inherent subjectivity of the method arising from lack of quantifiable, objective parameters in the evaluation of pulmonary sounds and shortcomings arising from limited frequency response of the stethoscope, it is regarded of low diagnostic value and its findings are further verified by other tests. Over the last 30 years, with the advancements in computer technology and digital signal processing field, the digital acquisition of pulmonary sounds with better sound transducers and computer hardware and the analysis of pulmonary sound waveform using advanced signal processing techniques have become an established research area. An extensive overview of pulmonary sound research is given in various review articles [20, 51, 65, 37]. The research on analysis of pulmonary sounds aims to parameterize sound data and correlate these parameters with common respiratory disorders.

The pulmonary sounds are believed to be produced due to air turbulence in the airways of the lungs although the exact mechanism of sound generation is still unknown. The changes in the lung structure that occur in some pathological conditions change the spectrum of sounds heard over the chest wall and may further cause the presence of additional abnormal sounds [20, 51, 65]. Pulmonary sounds are roughly divided into two classes, vesicular sounds (VSs) and adventitious sounds. VSs are the respiratory sounds heard over the chest wall and are synchronous with air flow in the airways. Their frequency spectra may change with the location of auscultation on the chest wall and with pathological conditions [21, 40, 59, 8]. Adventitious sounds, on the other hand, are additional sounds which usually occur with respiratory disorders. Both in literature and in this thesis, pulmonary sounds, respiratory sounds, lung sounds and breath sounds have been used interchangeably.

Crackles are discontinuous type of adventitious sounds that occur in pathological

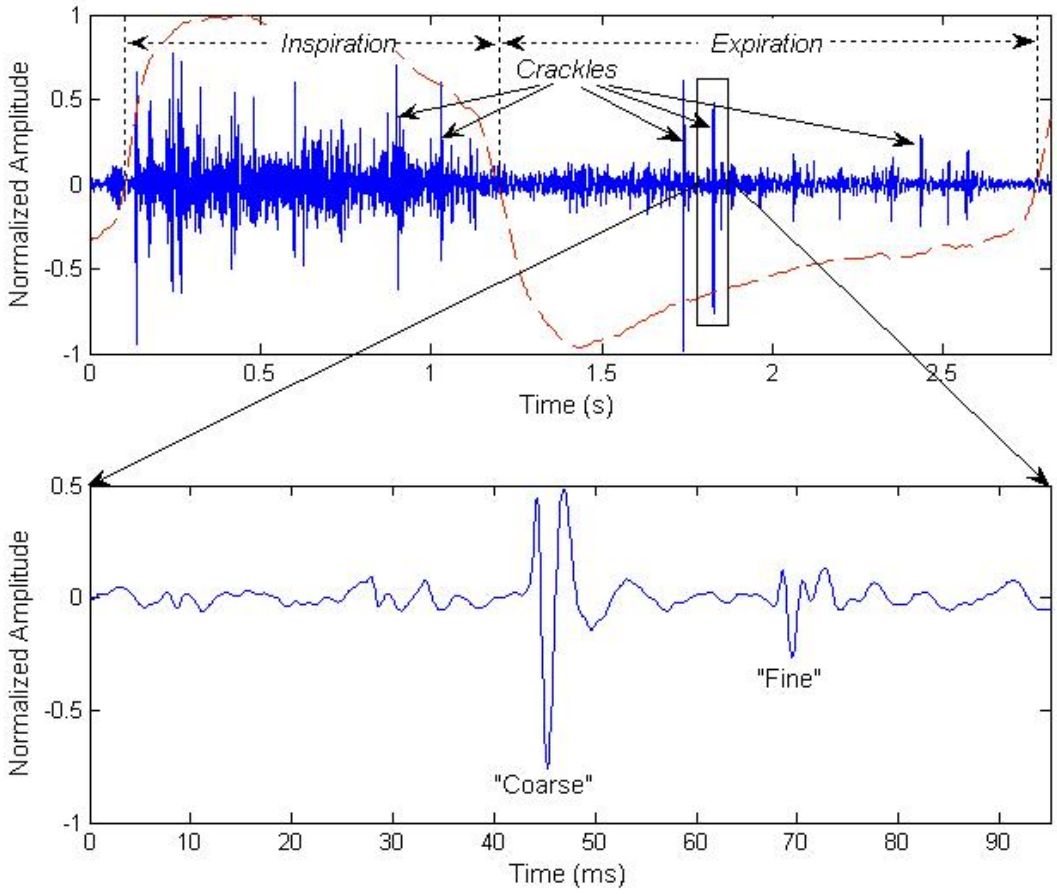

Figure 1.1 A phonopneumogram that presents lung sound and flow (dashed line) signals simultaneously. Crackles are superimposed upon VSs of a male patient with pneumonia. (b) Time expanded waveform of a part of the lung sound signal that includes CC and FC.

conditions and are superimposed on VSs (Figure 1.1). Crackles are explosive and transient in character, and occur frequently in cardio-respiratory diseases, being useful indicators in their diagnosis [17, 49, 19, 54]. Criteria for a crackle waveform have been suggested by Murphy et al. [47] as being a transient containing 3 to 16 baseline crossings with the amplitude of its largest peak greater than twice the amplitude of the background VSs. The waveform is expected to have a sharp onset deflection which is followed by deflections of progressively wider baseline crossings. The duration of a crackle is less than 20 ms and its frequency range is from 100 to 2000 Hz or even higher [20, 54]. The timing and pitch of crackles are usually correlated with diseases such as pneumonia, bronchiectasis, fibrosing alveolitis and asbestosis [49, 55, 66, 72, 53, 33, 69]. A typical crackle waveform may be depicted in Figure 1.1.

Crackles are generally classified as fine and coarse crackles according to their

Table 1.1
Representative crackle parameter values (ms) for fine and coarse crackle classes as suggested by different groups [13, 23, 24, 25, 26]. For comparison, Hoevers' set of parameters are converted to Murphy's using Eq. 4.1.

	Murphy		Hoevers		Munakata		ATS		CORSA
	IDW	2CD	IDW	2CD	IDW	2CD	IDW	2CD	2CD
Fine	0.5	3.3	0.8	4.0	1.0	4.40	0.7	<5	<10
Coarse	1.0	5.1	1.5	6.7	1.88	7.74	1.5	10	>10

duration and waveform, however a third class, medium, is occasionally used by some researchers [21, 34, 3, 27]. The discriminants between the crackle types are not obvious. There is a discrepancy among different groups in their classification of crackles. A crackle which is classified as fine according to one study may be classified as coarse according to another. This inconsistency is clearly seen in Table 1.1 where representative parameter values for two classes of crackles, namely coarse (CC) and fine (FC), as recommended by different groups, [47, 5, 26, 45, 64] are summarized. A crackle which is classified as coarse according to American Thoracic Society (ATS) definition, for instance, would be classified as fine according to Computerized Respiratory Sound Analysis Research Group ($CORSA$).

Crackles have been traditionally detected with stethoscopes in auscultation and this approach has been a source of great variability among observers. Interobserver disagreement on the assessment of crackles as either fine, medium or coarse was reported to be 53% among three observers in a work by Hudson et al. [27]. Similarly, in a study by Piirila et al. [56], agreement on the fineness and coarseness of crackles was around 60% among two observers. With the development of computerized systems for digitization and recording of pulmonary sounds mainly for pulmonary sound research, parameterization of crackles for a more objective description and classification have been attempted and various different sets of parameters have been used by different groups. Among these, the most popular have been two main studies by Murphy et al. [47] and Hoevers et al. [26]. In the study of Murphy et al., two parameters have been used to define crackles, mainly the Initial Deflection Width (IDW) which is the duration of the first deflection of the crackle and the Two-Cycle Duration ($2CD$) which

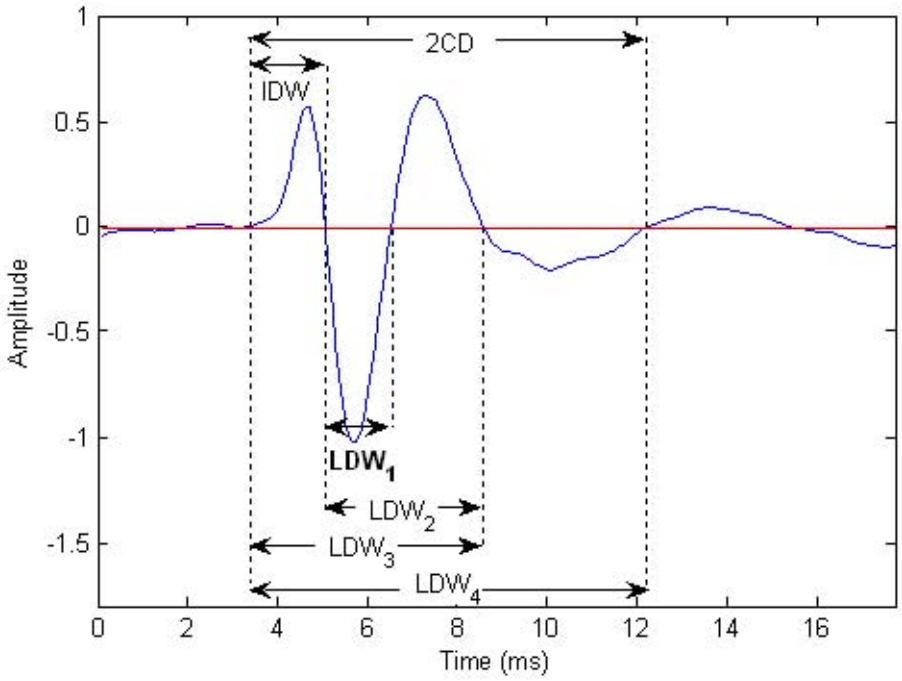

Figure 1.2 Commonly used parameters of crackles are shown on CC acquired from a patient with pneumonia. Two parameters defined by Murphy et al.: Initial deflection width (IDW) and two-cycle duration ($2CD$). Four parameters defined by Hoevers and Loudon: Largest deflection widths (LDW_{1-4}).

is the duration of the first two cycles of the crackle. Hoevers and Loudon, on the other hand, have preferred four parameters to classify crackles, mainly, Largest Deflection Width (LDW_1) which is the largest deflection of the crackle and the Widths of its First Three Right and Left Neighbors (LDW_{2-4}). The two types of parameterization are depicted in Figure 1.2. The parameters associated with quantization of crackles are exclusively time domain parameters based on zero-crossings of the waveform. These parameters do not bear information on the morphology of the waveform and suffer from background noise.

Crackles which are superimposed upon lung sounds are usually distorted with the background signal, especially in pathological conditions [32]. When parameters to characterize and quantify the morphology of crackles such as initial deflection width (IDW) or two-cycle duration (2CD) are extracted, the presence of background signal modulates the waveform of crackles such that the researchers are misled about the values of quantifiable crackle parameters. The finer the crackle is, the stronger the

effect of the artifact will be. To analyze crackles more accurately, the background signal which is mainly the VSs should be eliminated. However there is no a-priori information on the frequency band of the background signal which is affected by the type of pathology of the lung, by the phase of the occurrence of the crackle within the respiratory cycle and by the location of the recording microphone and of the crackle which has a wide frequency range. Moreover, the frequency components of crackles which range from 100 Hz to 2 kHz and the frequency spectra of background lung sounds which concentrate up to 250 Hz overlap [65]. There have been studies on the elimination of VSs [50, 23, 42, 41] but the aim of these studies was to detect the presence of a crackle waveform without taking crackle waveform distortion into consideration.

In this study, the aim is to study the characteristics of pulmonary crackles with a view to find the optimum number of clusters and to find the boundaries between the clusters that correspond to defining the characteristics of each crackle type. To this end, an algorithm to eliminate the VSs with minimal distortion of crackle waveform is developed. Then, wavelet networks have been employed to automatically depict the crackle waveform with only a small set of meaningful parameter values as is necessary for typical discrimination tasks. The parameters extracted from the parameters obtained from the wavelet network have been used along with the traditional parameters in clustering experiments based on maximum likelihood, Expectation-Maximization (EM) algorithm to probe the question of whether a third type of pulmonary crackles does exist and also what the typical crackle parameter values for each type are.

The database, in this study, consisted of nearly three thousand crackles recorded from thirteen different subjects with various pulmonary disorders. These sounds were acquired from fourteen different microphone locations on the posterior chest wall of each subject.

In Chapter 2, a filtering method is proposed for VS elimination based on the estimation of cut-off frequency for each crackle such that the waveforms of crackles will be minimally distorted by the filtering operation while VSs are optimally eliminated. To achieve a minimal distortion in the crackle waveforms, a distortion metric is defined

on the correlation between waveforms in raw and filtered signal. The optimal cut-off frequency is estimated by an iterative process while the distortion metric is used as the factor to determine where the process should be stopped. After determining an optimal cut-off frequency for each crackle, a regression analysis is employed to predict the cut-off frequency with respect to the spectral components of crackles to reduce computational cost especially for online processes.

In Chapter 3, the filtered crackle waveforms are modeled using wavelet networks (WNs). Wavelets are useful for the interpretation of transient signal since they have finite energy concentrated in a time interval. Moreover, the wavelet families that are used in the interpretation can be selected according to the characteristics of the target signal. The WNs give the opportunity to interpret the target signals using wavelets by an iterative process. WN used in the study has a neural network structure with a single hidden layer that employs the wavelets in their hidden nodes as transfer function. The complex Morlet (cM) wavelet is selected for modeling since its waveform is similar to the crackle waveform and is flexible for the iterative modeling process. Due to the relative simplicity of the crackle waveform, WNs with up to two hidden nodes are adequate for modeling. Single-node WN interprets the high-energy components of crackle waveform whereas double-node WN models the expanding waveform of the crackle with lower error. The conventional parameters of crackles are defined on the zero-crossings of the crackle waveform whereas the WNs yields parameters that both interpret the crackles in time-frequency domain and contains the information for a faithful regeneration of the modeled crackle waveforms.

The clustering analysis of crackles in the feature spaces that are constructed using conventional and WN parameters is described in Chapter 4, where the existing discrepancy in the crackle literature on the characteristics of crackle types and even on the number of crackle types is probed. In the studies related with crackle classification, the crackles are labeled according to the auditory perception of the observers. The subjectivity in the labeling analysis causes the differences in the typical parameters of crackle types even if the number of crackle types is accepted as two. To overcome this subjectivity problem, an unsupervised classification method is employed

to determine the optimal number of crackle types and their parametric characteristics. Expectation-Maximization (EM) method is used to cluster the crackle distribution on the parametric spaces such that the data is assumed to be generated by Gaussian mixture densities and therefore each crackle type to distribute normally in parametric spaces. Therefore, the labels of crackles and the parameters of crackle clusters that maximize the likelihood of the data are determined as optimal for the selected number of crackle types. Bayesian Inference Criterion (BIC) and Akaike Information Criterion (AIC) are used as indicators to determine the optimum number of crackle types. The results provide supportive evidence for the existence of a third crackle type, medium, in addition to the commonly-used two types, i.e. fine and coarse.

The main contributions of this thesis are outlined below:

- A new preprocessing and filtering algorithm based on a distortion metric is proposed and tested on the simulated crackles with an aim to remove the vesicular sounds from the crackle waveforms.
- A new approach to parameterize pulmonary crackles is proposed in which wavelet network modeling of pulmonary crackles is employed, using Morlet wavelets for the first time for this signal. The features extracted from this model are used to represent pulmonary crackles, exhibiting a distinctly different approach from the conventional methods based on zero-crossings of the crackle waveforms. Consequently, new parameter sets for crackle representation are proposed.
- An unsupervised classification of crackles is realized for the first time. To this effect, clustering analysis based on expectation maximization method is implemented on real data.
- The existence of a third crackle type, namely medium, is tested for the first time using the clustering experiments. The validation of its existence is realized for the first time, using both the conventional parameters and the proposed parameters of this study.
- The mean values of all features of five different parameter sets of different crackle

types for both two and three-type cases have been defined, for the first time, based on the results of the clustering experiments.

The complementary studies explained in the three chapters render new opportunities for computer-based analysis of pulmonary sounds based on crackles. The crackles representing crackle types can be generated using parameters of wavelet modeling and can be used as crackle atoms for detecting on the pulmonary sound signal using matching pursuit method. The models can be fine-tuned on the detected crackle waveforms in order to interpret the waveform with minimal error. Therefore, we can determine the crackle characteristics of the pulmonary sound signal, i.e. the pitch, numbers and the location on the respiratory cycle of crackles. Using the advantages of simultaneous acquisition of the pulmonary sounds using the multi-channel DAQ system, the localization and severity of pulmonary disorders in the thorax can be estimated. Conclusions drawn in this study are detailed in Chapter 5.

2. ELIMINATION OF VESICULAR SOUNDS FROM PULMONARY CRACKLE WAVEFORMS

Pulmonary crackles and their parameters are very useful in the diagnosis of pulmonary disorders. A new automatic method has been proposed for the elimination of background VSs from crackle signal with a view to introduce minimum distortion to crackle parameters. A region of interest (ROI) is designated and a distortion metric based on the correlation between raw and filtered waveforms in that region is defined. Filter cut-off frequency is estimated based on the distortion metric. To reduce computational cost, a regression analysis is also realized which predicts a new fitted cut-off frequency from the estimated cut-off frequency. As a comparison basis, wavelet filtering is also applied on the same data. The algorithm is validated on simulated crackles superimposed on recorded VSs with results indicating that filtering is achieved with minimal distortion of crackle parameters. The algorithm is also applied on real crackles from subjects with various respiratory disorders. The results show the extent of the effect of VSs on crackle parameters, emphasizing the significance of proper filtering in crackle studies.

In Section 2.1, the material including the data acquisition system, the database of real crackles used and the description of simulated data are presented. The methodology and the evaluation metrics used in building filters are given in Section 2.2 while results are presented in Section 2.3.

2.1 Material

Fourteen air-coupled electret microphones (SONY ECM44-BPT) placed on the posterior chest wall and a pneumotachograph (Validyne CD379) were used to record the pulmonary sounds and the airflow simultaneously in order to synchronize on the inspiration-expiration phases. Low-noise preamplifiers, 8th order Butterworth low-

Figure 2.1 The components of the DAQ System, i.e. 14 air-coupled microphones, a box containing amplifiers and filters, a flow-meter and DAQ Card embedded in a laptop computer.

pass filters with 4 kHz cut-off frequency and 6th order Bessel high-pass filters with 80 Hz cut-off frequency were used in order to minimize frictional noise and heart sound interference with minimal phase distortion and for an anti-aliasing filter. The preprocessed signals were digitized with a 12-bit ADC Card (National Instruments DAQCard-6024E) at a 9.6 kHz sampling rate and stored by means of a notebook computer (DELL Inspiron 2650). The DAQ system is depicted in Figure 2.1 and described in detail in Sen and Kahya [63].

These records were acquired at Istanbul University Cerrahpasa Medical School and Yedikule Teaching Hospital for Chest Diseases and Thoracic Surgery by members of our laboratory with the guidance of a physician specialized in pulmonary medicine. Informed consent was taken from the subjects before recordings. The lung sounds were acquired from 13 subjects with obstructive and/or restrictive respiratory disorders. From these records, 2811 crackles were visually detected from time expanded waveform [47] of lung sounds by two independent observers for filtering experiments. The database of crackles consisted of a wide range of crackle frequencies from coarse to fine.

Simulated crackles were also used to verify the performance of the proposed filtering method. Two crackles representing FCs and CCs are generated with a function defined by Kiyokawa et al. [34] such that crackle waveform ($y(t)$) is defined as a product of a progressively wider sinusoidal function ($y_0(t)$) and a modulating function ($m(t)$) that concentrates energy at the beginning of crackle waveform:

$$y(t) = m(t)y_0(t) \tag{2.1}$$

$$m(t) = 0.5(1 + \cos[2\pi(t^{0.5} - 0.5)]) \tag{2.2}$$

$$y_0(t) = \sin(4\pi t^{\alpha}) \tag{2.3}$$

where $\alpha = \log(0.25)/\log(t_0)$ and t_0 is first zero-interception time of crackle waveform that may be interpreted as the ratio of $IDW/2CD$. Simulated crackles have two cycles and their parameters are determined according to Sovijarvi et al. [64] such that FC has (IDW: 1ms, $2CD$: 5ms) or (LDW_1: 1.23ms, LDW_4: 5ms) and CC has (IDW: 2ms, $2CD$: 10ms) or (LDW_1: 2.47ms, LDW_4: 10ms). The crackle simulation function and the simulated crackles crackles are depicted in Figure 2.2.

Simulated crackles are superimposed on VSs recorded from 31 healthy nonsmoking subjects with no reported pulmonary disease history. Subjects are maneuvered such that they breathe with a flow rate of approximately 1 L/s. Single respiratory cycle that consists of an inspiratory and an expiratory phase is used for each healthy subject. The cycle is divided into 256-sample non-overlapping segments and CC and FC are superimposed on each VS window separately. This approach guarantees that both FC and CC are superimposed at each subphase (early, mid and late inspiration and expiration) of VS. The 256-sample VS window that crackle is superimposed on is defined as "crackle window (CW)". The same terminology is used for the extracted pathological lung sound window that includes a real crackle.

The relative amplitude of superimposed crackles with respect to background VS is determined according to the threshold of hearing for broadband masking noise.

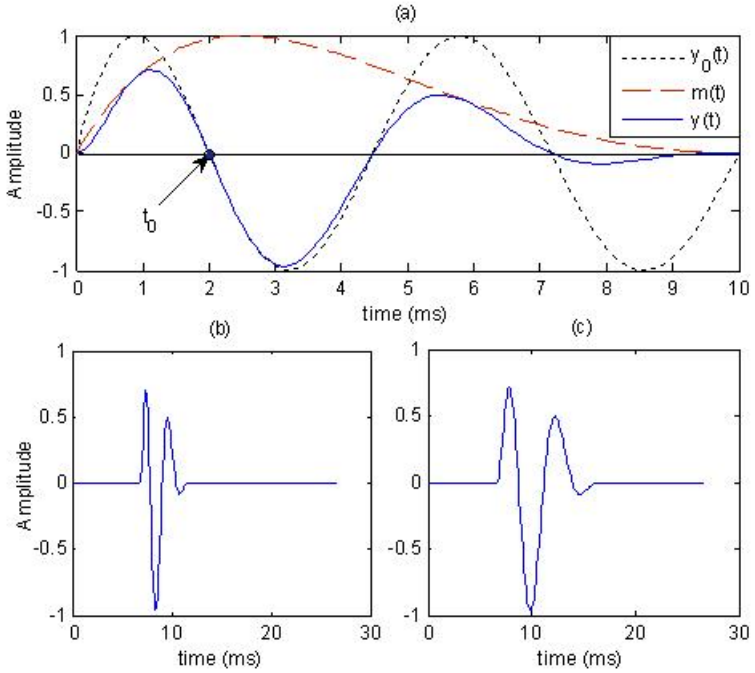

Figure 2.2 (a) Components of a generated CC. A crackle ($y(t)$: solid line) is the product of a progressively wider sinusoidal function ($y_0(t)$: dotted line) and modulating function ($m(t)$: dashed line) where t_0 is a parameter for controlling the ratio of $IDW/2CD$ and the morphology of the generated crackle. (b) $FC \rightarrow IDW$: 1ms and $2CD$: 5ms. (c) $CC \rightarrow IDW$: 2ms and $2CD$: 10ms.

According to psychoacoustics [77], the frequency components of test sounds should be approximately 20 dB higher than those of masking noise for frequencies less than 1 kHz. A similar understanding is used in Murphy's definition of crackles in relation to VS [46]. Accordingly, we applied a novel method in superimposing crackles on VS such that for each window the average power of the simulated crackle at its 3dB (or half power) bandwidth is 20 dB higher than that of VS at the same frequency interval. The VS elimination method was written in the MATLAB® programming environment (Version 7.3.0 (R2006b)) and was implemented on an Intel® Pentium® D 3.0 GHz Processor.

2.2 Methodology

The method for filtering the VSs from the crackle signal comprises of first selecting the region of interest for each crackle, then estimating f_c for each crackle

based on the defined distortion metric and finally filtering each crackle with the f_c^{est}. In order to reduce the computational cost in estimating f_c for each crackle, a curve fitting algorithm using $cPS_{\%}$ of each crackle is applied to predict f_c with minimum error, namely, f_c^{fit}. The method is applied on both data set of real crackles and that of simulated crackles superimposed on recorded VS.

Crackles in a respiratory cycle belonging to the same subject usually have different durations and frequency content therefore f_c of the high-pass filter applied on each crackle in the proposed method depends on spectral characteristics of that crackle. It is particularly important that a standard rule is used in defining the location and the boundaries of the crackle to be filtered. ROI of CW is defined to be used in the power spectral estimation and distortion calculation by considering that ROI should include $2CD$ of a crackle that is equivalent to LDW_4. The peak of LDW_1 of a crackle is used as the reference point for selection of ROI. This reference point renders the automatic processing of the crackle possible once it is detected [26]. Due to the presence of background vesicular signal, the use of zero-crossings as reference points may be misleading thus local minima and local maxima, known as local extrema, are considered in order to select start-end points of ROI. The second extremum before and the third extremum after the peak of LDW_1 are appointed as the start-end points of a region that includes $2CD$. The selection of the ROI is depicted in Figure 2.3. ROI is determined from raw CW before filtering and the same region is used for the filtered CW.

The main criterion in selecting f_c for the high-pass filter of a crackle is to introduce minimum distortion to the shape of the crackle waveform during filtering. Consequently a distortion metric is defined and the frequency domain is scanned in ascending order until the designated distortion threshold (DT) amount in crackle waveform is reached.

The distortion metric chosen for this method is related to the correlation coefficient (R_{x_r,x_f}) between crackle waveforms in raw and filtered signals. For N-length raw

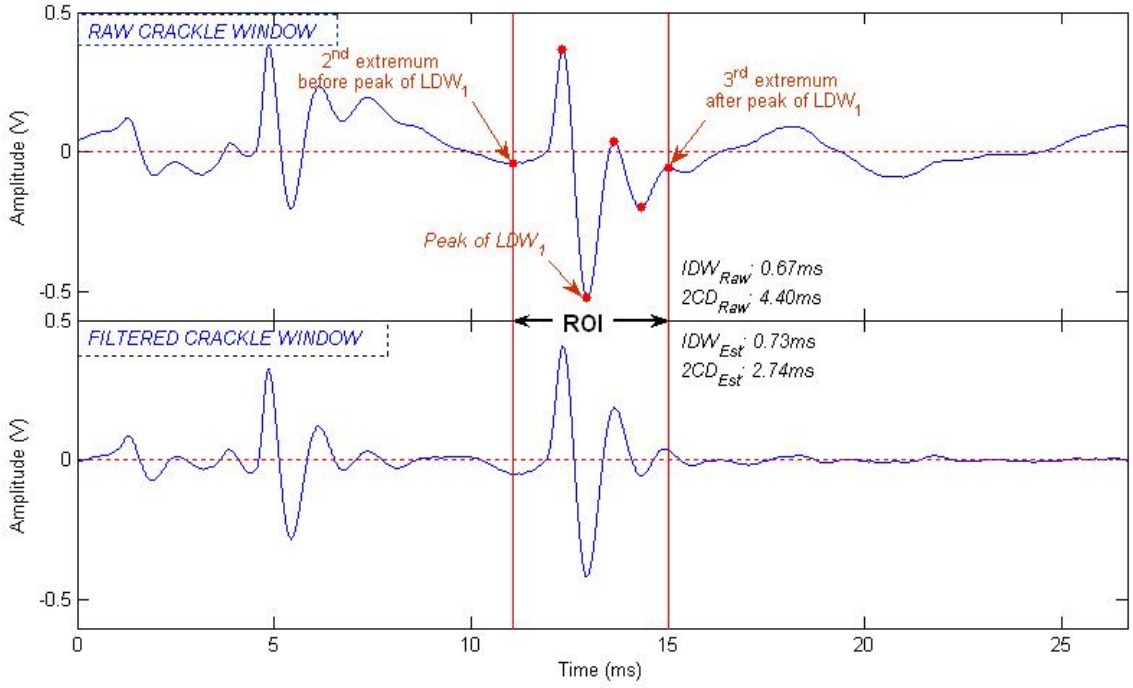

Figure 2.3 Region of interest (ROI) for the calculation of distortion amount. ROI is between 2nd extremum before and 3rd extremum after peak of LDW_1.

(x_r) and filtered (x_r) signals, R_{x_r,x_f} is defined as

$$R_{x_r,x_f} = \frac{\sum_{n=0}^{N-1}(x_{r,n} - \hat{x}_r)(x_{f,n} - \hat{x}_f)}{(N-1)s_r s_f} \tag{2.4}$$

where $\hat{x}$ is the mean, $\hat{x} = (1/N)\sum_{n=0}^{N-1} x_n$, and s is the standard deviation, $s = [(1/(N-1))\sum_{n=0}^{N-1}(x_n - \hat{x})^2]^{1/2}$.

Since the same intervals of samples from raw and filtered signal are used to calculate R_{x_r,x_f}, filtering should not yield a phase distortion. To accomplish zero-phase filtering, the output of filter is reversed and filtered again. A 6^{th} order digital high-pass Butterworth filter is used since its flat frequency response and its order is convenient for supplying slope greater than $18dB.oct^{-1}$ [68]. The forward-backward process doubles the filter order [43]. The process of taking the correlation coefficient inherently filters out the dc component of the signals. Moreover the contribution of differences in zero crossings which are in fact significant in case of crackle parameters is much less than that of higher amplitudes. To enhance the contribution of zero-crossing,

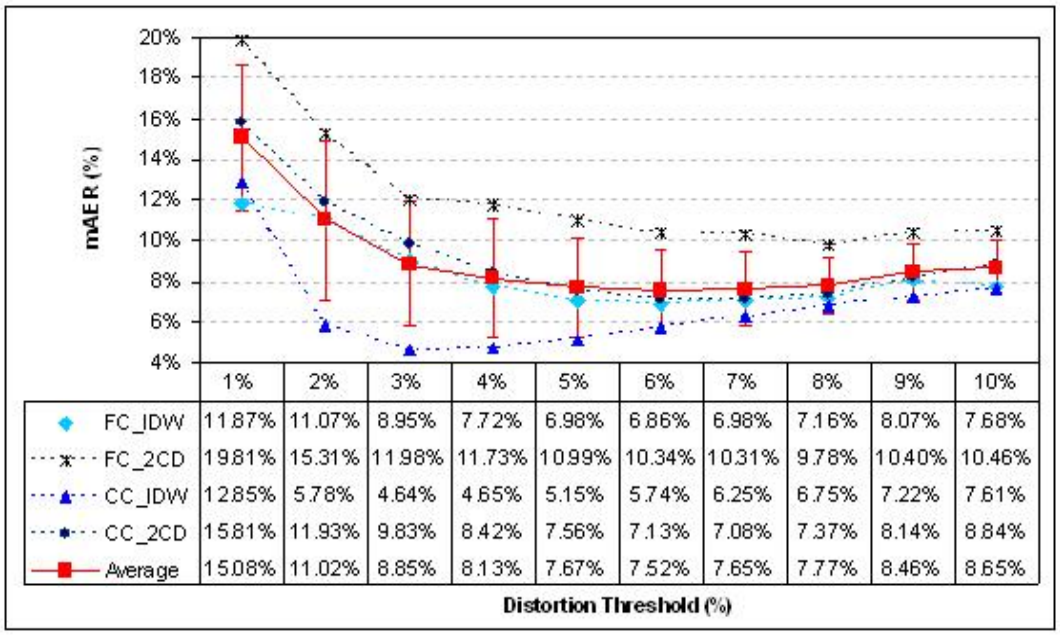

	1%	2%	3%	4%	5%	6%	7%	8%	9%	10%
FC_IDW	11.87%	11.07%	8.95%	7.72%	6.98%	6.86%	6.98%	7.16%	8.07%	7.68%
FC_2CD	19.81%	15.31%	11.98%	11.73%	10.99%	10.34%	10.31%	9.78%	10.40%	10.46%
CC_IDW	12.85%	5.78%	4.64%	4.65%	5.15%	5.74%	6.25%	6.75%	7.22%	7.61%
CC_2CD	15.81%	11.93%	9.83%	8.42%	7.56%	7.13%	7.08%	7.37%	8.14%	8.84%
Average	15.08%	11.02%	8.85%	8.13%	7.67%	7.52%	7.65%	7.77%	8.46%	8.65%

Figure 2.4 The mean of absolute error rates ($mAER$s) between crackle waveform parameters after filtering and their reference values. AERs are calculated for the parameters of both FC and CC according to 1%-10% DTs.

the absolute values of raw and filtered signals in the respective ROIs are taken before the calculation of the correlation coefficient. The distortion metric, D, is defined as

$$D(\%) = (1 - R_{x_r,x_f}) \cdot 100\% \tag{2.5}$$

A lower limit for the correlation coefficient is calculated using the simulated crackles whose parameters are known. To include all phases, a complete healthy respiratory cycle is divided into 256-sample segments where the number of segments is 70. Simulated FCs and CCs are superimposed on each segment as described before. The absolute error rates (AERs) between parameters of simulated (p_{Ref}) and filtered (p_i) crackles are used to indicate the performances of different DTs. AER is defined as

$$AER(\%) = \frac{|p_i - p_{Ref}|}{p_{Ref}} \cdot 100\% \tag{2.6}$$

where $|.|$ represents the absolute value.

Mean values of AERs ($mAER$s) are calculated for IDW and $2CD$ parameters of FC and CC and the common performance of DTs are evaluated by taking the

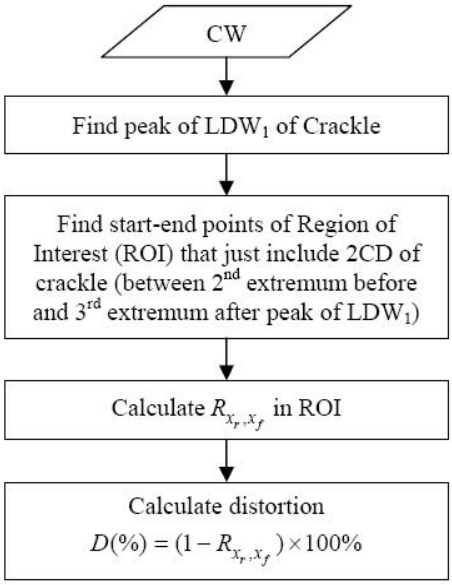

Figure 2.5 Block diagram for the calculation of the distortion metric

average of $mAER$ results. The reference values (p_{Ref}) for IDW and $2CD$ of FC are 1ms and 5ms, respectively, whereas those of CC are 2ms and 10ms, respectively. The best performance (minimum $mAER$) is reached at 6% and 8% DTs for IDW and $2CD$ of FCs whereas at 3% and 7% DTs for IDW and $2CD$ of CCs. The best common performance is reached at 6% DT at which averaged $mAER$ is minimum and therefore 6% DT is used as the optimum threshold for the determination of f_c resulting in a lower limit of 0.94 for the correlation coefficient. The graphs of mean of absolute error rates for crackle waveform parameters versus DT values are depicted in Figure 2.4. The block diagram for the calculation of the distortion metric, D, is depicted in Figure 2.5.

Instead of scanning frequency domain with a constant step-size where the spectral attributes of the crackle are not considered, the step size is determined according to the cumulative power spectrum (cPS) of ROI. The $cPS_{\%}$ are employed as cut-off frequencies with a 1% step size, therefore, the higher the power of ROI at a frequency interval is, the smaller an increase in f_c will be at frequency domain. Thus the resolution of the step-size is increased at frequencies where the spectral components of a crackle exhibit higher power. cPS is defined as normalized cumulative summation of power spectral density (PSD) that is estimated for N-length sequence $x_0, x_1, \ldots, x_{N-1}$

using periodogram method as

$$PSD(jw) = (1/N)|\sum_{n=0}^{N-1} x_n e^{-jwn}|^2 \tag{2.7}$$

$$cPS(jw_k) = \sum_{n=0}^{k} PSD(jw_n) / \sum_{n=0}^{M-1} PSD(jw_n) \tag{2.8}$$

where M equals to $(N/2)+1$ or $(N+1)/2$ for even or odd N, respectively.

Since PSD indicates the power of the data sequence at a particular frequency, cumulative power spectrum indicates the proportion of the energy up to a certain frequency to total energy. In the algorithm for the estimation of f_c, $cPS_{\%}$s are tested in ascending order until DT is reached. The highest $cPS_{\%}$ at which the distortion amount is less than DT is appointed as f_c^{est} for the CW. The procedure for f_c estimation is presented in Figure 2.6.

The algorithm described above is applied on each crackle separately. Computational cost of determination of f_c may be too high in real-time applications which may involve further processing of lung sound data. Thus a compromise may be justified where a lower computational cost with higher distortion is achieved. Therefore repetitive filtering operation of the crackle waveform by scanning $cPS_{\%}$ until DT is reached may be avoided if a relationship between optimum f_c and $cPS_{\%}$ is found. The search for this relationship is carried out by exploring the minimum error between the f_c^{est} and the f_c^{fit} as given below.

Since the relationship between f_c^{est} and $cPS_{\%}$ may be curvilinear, polynomial regression models are carried out to fit this relationship. A response variable (y) may be expressed using P^{th}-degree polynomial in one independent variable (x) as

$$y = \sum_{p=0}^{p} \beta_p x^p + \varepsilon = \hat{y} + \varepsilon \tag{2.9}$$

where β_p is the unknown regression coefficient, ε is the residual and $\hat{y}$ is the fitted value. In our problem, x, y and $\hat{y}$ substitute $cPS_{\%}$, f_c^{est}, and f_c^{fit} respectively. In

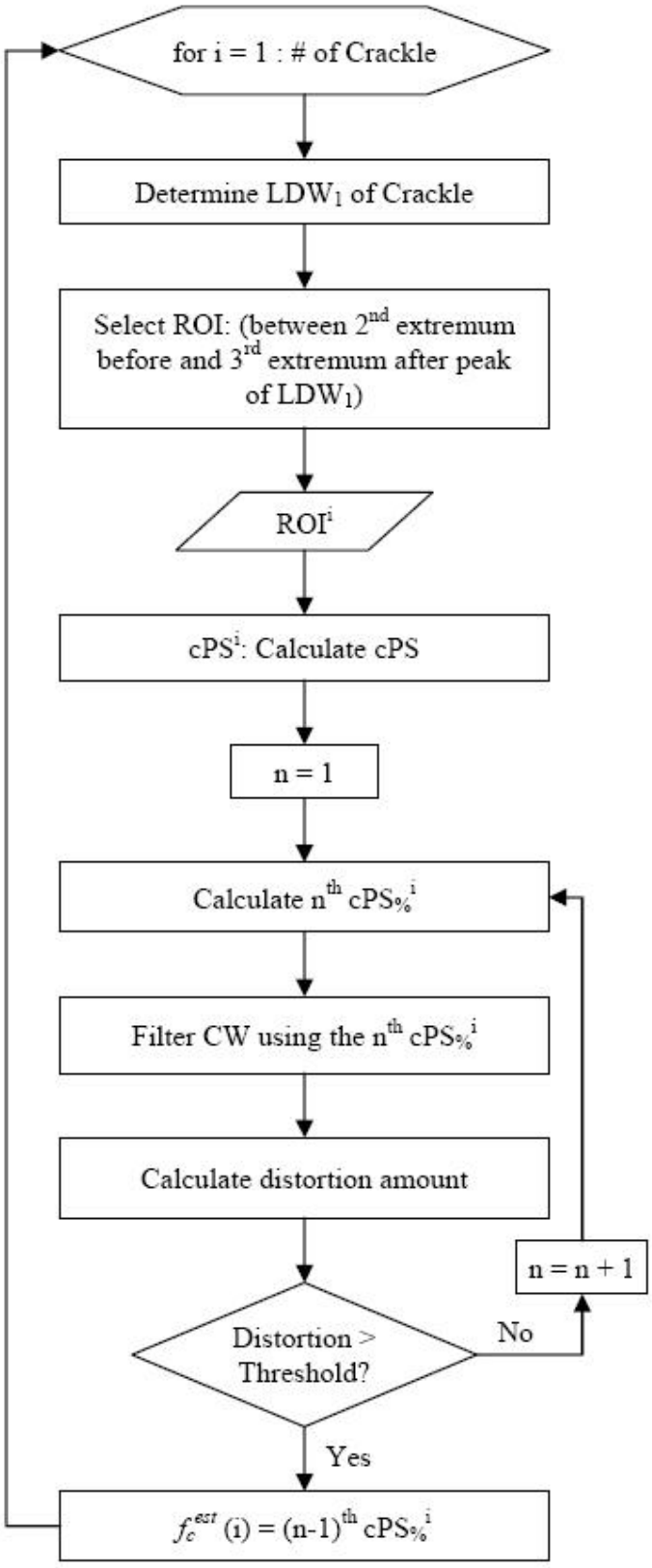

Figure 2.6 Block diagram for f_c estimation

regression analysis, β_p is estimated using the least squares method such that the sum of the residuals (E) is minimized. E is defined for N samples as

$$E = \sum_{i=1}^{N} \varepsilon_i^2 \tag{2.10}$$

$$\varepsilon_i = y_i - \hat{y}_i = y_i - \sum_{p=0}^{p} \beta_p x^p \tag{2.11}$$

To determine the optimum degree of the polynomial, coefficient of multiple determination (R^2) that is defined as the ratio between the regression sum of squares (SS_R) and the total corrected sum of squares (SS_T) is used as global statistics to assess the model fitting [44],

$$R^2 = SS_R/SS_T = 1 - SS_E/SS_T \tag{2.12}$$

$$SS_T = \sum_{i=1}^{N} (y_i - \bar{y})^2 \tag{2.13}$$

$$SS_R = \sum_{i=1}^{N} (\hat{y}_i - \bar{y})^2 \tag{2.14}$$

where $SS_E = \sum_{i=1}^{N} (y_i - \hat{y}_i)^2$ is the error sum of squares, $\hat{y}$ is predicted value and $\bar{y}$ is grand mean.

Although the adjusted form of coefficient of determination (R^2_{adj}) is generally preferred to penalize the increase in the degree of polynomials using the degrees of freedom as divisor of sum of squares in calculation of statistic, it can only work ideally for small sample size. However the decrease in the error degrees of freedom ($n - p$) by increasing the model order causes very small changes in R^2 statistic when sample size is large ($n \gg p$). R^2_{adj} is calculated as

$$R^2_{adj} = SS_R/SS_T = 1 - \frac{SS_E/(n-p)}{SS_T/(n-1)} \tag{2.15}$$

where n and p are the number of samples and the polynomial degree in regression, respectively. The total and error degrees of freedom are $(n-1)$ and $(n-p)$, respectively. In our problem, n is 11192 and 2811 for simulated and real crackles whereas p changes in the range $1-8$.

R^2 is calculated for the $1^{st}-20^{th} cPS_{\%}$ using the $1^{st}-8^{th}$ degree polynomials, as depicted in Figure 2.7. The regressions for all eight polynomials have the maximum R^2 statistic at the 3rd $cPS_{\%}$ for both simulated and real crackles. R^2 statistics at $3^{rd} cPS_{\%}$ are depicted according to polynomial degree in the small windows in Figure 2.7 and the knee of curves is at 3^{rd} and 4^{th} degree polynomials for simulated and real crackles, respectively. Therefore, the cut-off frequencies that are predicted based on 3rd $cPS_{\%}$ using 3^{rd} and 4^{th} degree polynomials are used to reduce the computational cost of the filtering algorithm.

To compare the proposed VS elimination algorithm with a familiar method, wavelet filtering is also performed on both simulated and real data. For optimum performance, the correlation between wavelet waveform and crackles should be high therefore 3^{rd} order Daubechies' wavelet with six-coefficient filters is used as the mother wavelet in multi-resolution analysis of CWs. Since its asymmetric and sharp-deflecting waveform resembles the crackle waveform, this wavelet was used in a previous study on crackle detection carried out in our laboratory [58].

To address the main frequency components of VS within the *0-200* Hz band, the 5^{th} level discrete wavelet decomposition is applied on the CWs with frequency components between *0-4800* Hz. Therefore, the signal is decomposed into six wavelet components within the frequency bands: *2400-4800* Hz, *1200-2400* Hz, *600-1200* Hz, *300-600* Hz, *150-300* Hz, and *0-150* Hz. To remove the wavelet components within a frequency band including major VS components, a null-vector is replaced with the wavelet component in the reconstruction of the signal. The simulated CC and FC are employed to evaluate the performance of the methods. The peak frequencies of simulated CC and FC are 200 Hz and 400 Hz, respectively and the half-power bands of CC and FC are *135-270* Hz and *270-540* Hz, respectively. Thus the 6th wavelet

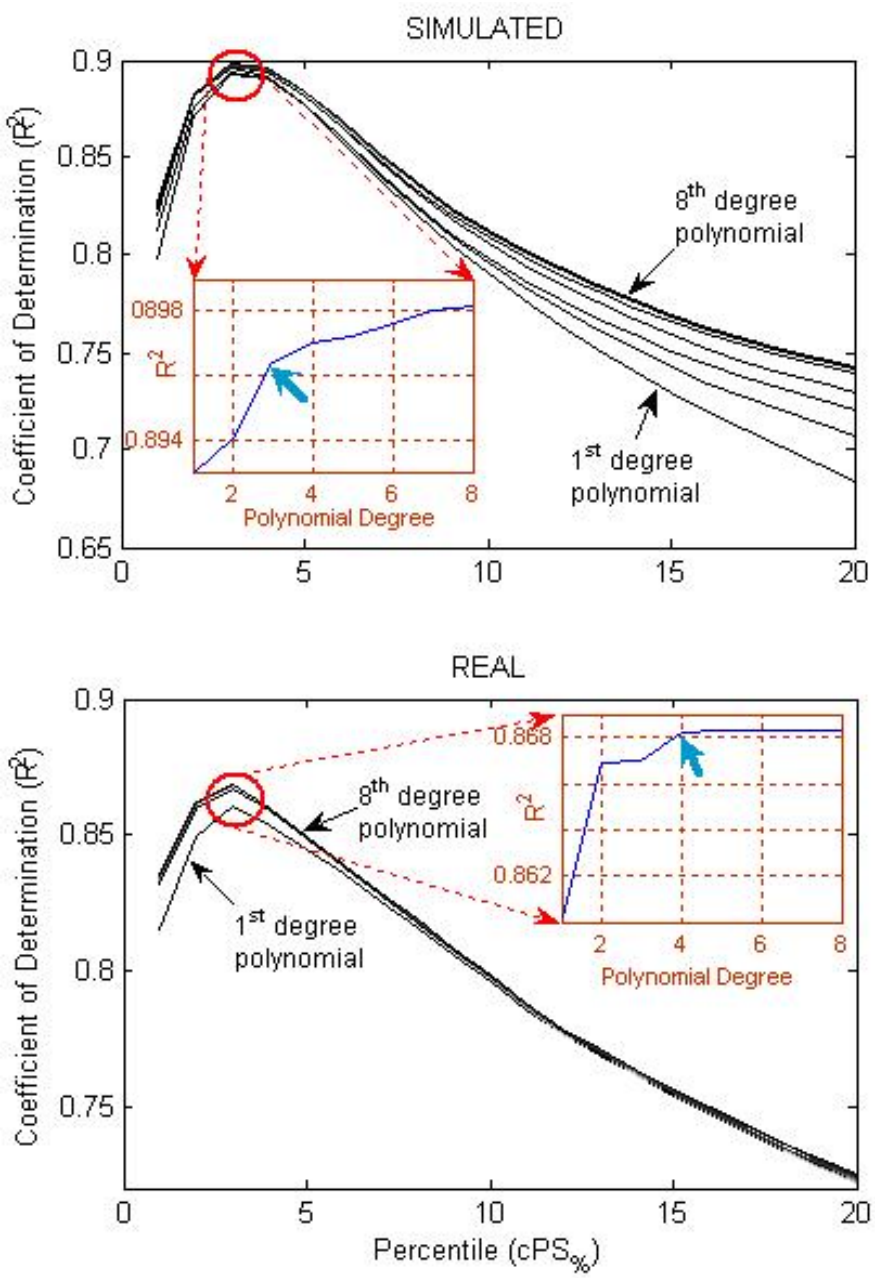

Figure 2.7 Coefficient of determination (R^2) of regression analysis using 1st-8th degree polynomials according to $cPS_{\%}$ of simulated and real crackles. The peaks of the R^2 curves are at the 3rd $cPS_{\%}$ for both simulation and real crackle analysis. R^2 of all eight polynomials at the 3rd $cPS_{\%}$ is depicted in the small figures. The knees of the curves are at the 3rd and 4th degree polynomials for simulated and real crackles, respectively.

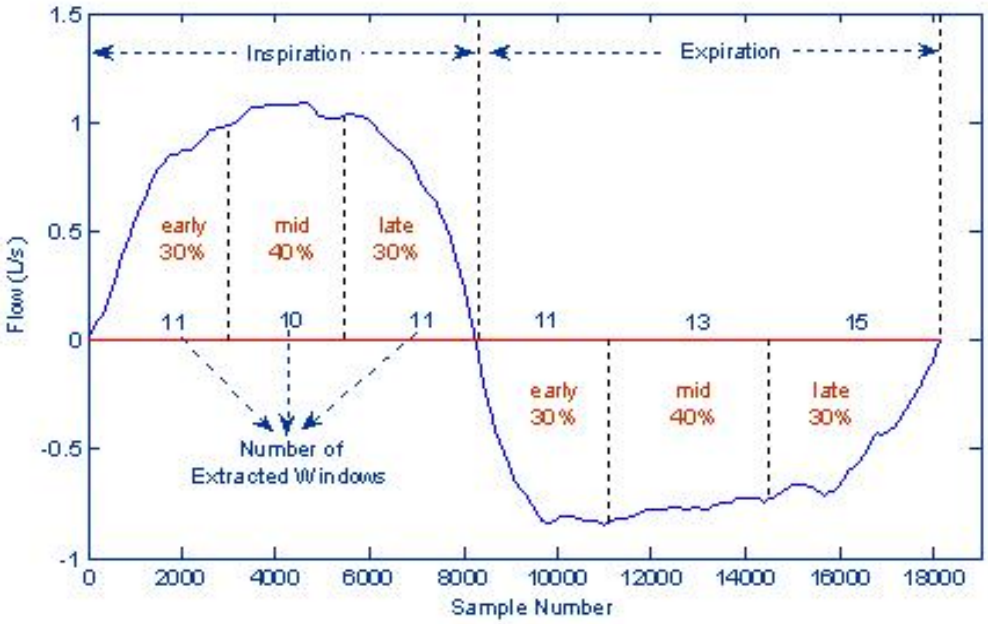

Figure 2.8 Subphases of a respiratory cycle. The semi-cycles of a respiratory cycle, i.e. inspiratory and expiratory cycles, are divided into three clinical sub-phases, i.e. early, mid and late, according to the amount of inspired or expired volume corresponding to the area under the flow curve. The numbers of extracted windows of each sub-phase are shown for this flow curve.

component within *0-150* Hz band overlaps with the frequency component of simulated CC. In wavelet component elimination, 6^{th} wavelet components are removed and the variation in the crackle waveform is observed. To evaluate the performance of wavelet filtering, absolute error rates (AERs) on crackle parameters are calculated.

2.3 Results

The quantitative evaluation of the proposed algorithm is first performed on simulated crackles of known parameters. Results for both filters with f_c^{est} and f_c^{fit} are obtained and compared with results of wavelet filtering. After the verification on simulated data, the algorithm is applied on recorded data set of crackles which are already distorted with VSs with untraceable true parameter values. Consequently, instead, the changes in scatter plots of real crackle parameters are demonstrated. As a final step, a sensitivity analysis of crackle parameters to filter cut-off frequencies is carried out with an aim to justify the purpose of this study.

Table 2.1
Number of VS segments used as background sounds for simulated crackles

Inspiration			Expiration		
Early	Mid	Late	Early	Mid	Late
939	795	917	867	872	1206

In evaluating the VS elimination algorithm, simulated crackles of known parameters, which are superimposed on different temporal phases of a respiration cycle and are therefore distorted, are used. Two types of crackles are simulated and superimposed on VSs of a full cycle from each subject. Since timing of crackles in a respiratory cycle is one of the main characteristics of pulmonary disorders in diagnosis, the results are classified according to the clinical sub-phases, i.e. early, mid, late inspiration and expiration. These phases are defined according to the inspired and expired air volume during respiration corresponding to the area under the flow curve in our study, representing complementary 30%, 40% and 30% portion of the respired air volume, respectively. The definitions of subphases of a respiration cycle are depicted in Figure 2.8. The number of VS segments used for background signal for simulated crackles of each respiratory subphase is given in Table 2.1.

The VSs are divided into non-overlapping 256-sample segments and crackles are located at the end of the first quarter of each window. The results from simulated crackles consist of two parts i.e. for f_c^{est} and f_c^{fit}. The simulated FC has an IDW of 1 ms and $2CD$ of 5 ms whereas the simulated CC has an IDW of 2 ms and $2CD$ of 10 ms. The waveforms and their corresponding frequency spectra at each step of the proposed algorithm are depicted in Figure 2.9 and 2.10.

f_c^{est} is obtained using the DT defined on each crackle. To lower the computational cost, filtering is also performed using the fitted cut-off frequencies. Wavelet filtering is also applied on the same data for a comparison basis. Each algorithm is quantitatively evaluated by comparing the values of the true crackle parameters, i.e. IDW and $2CD$, with those of superimposed (raw) crackles that have undergone dis-

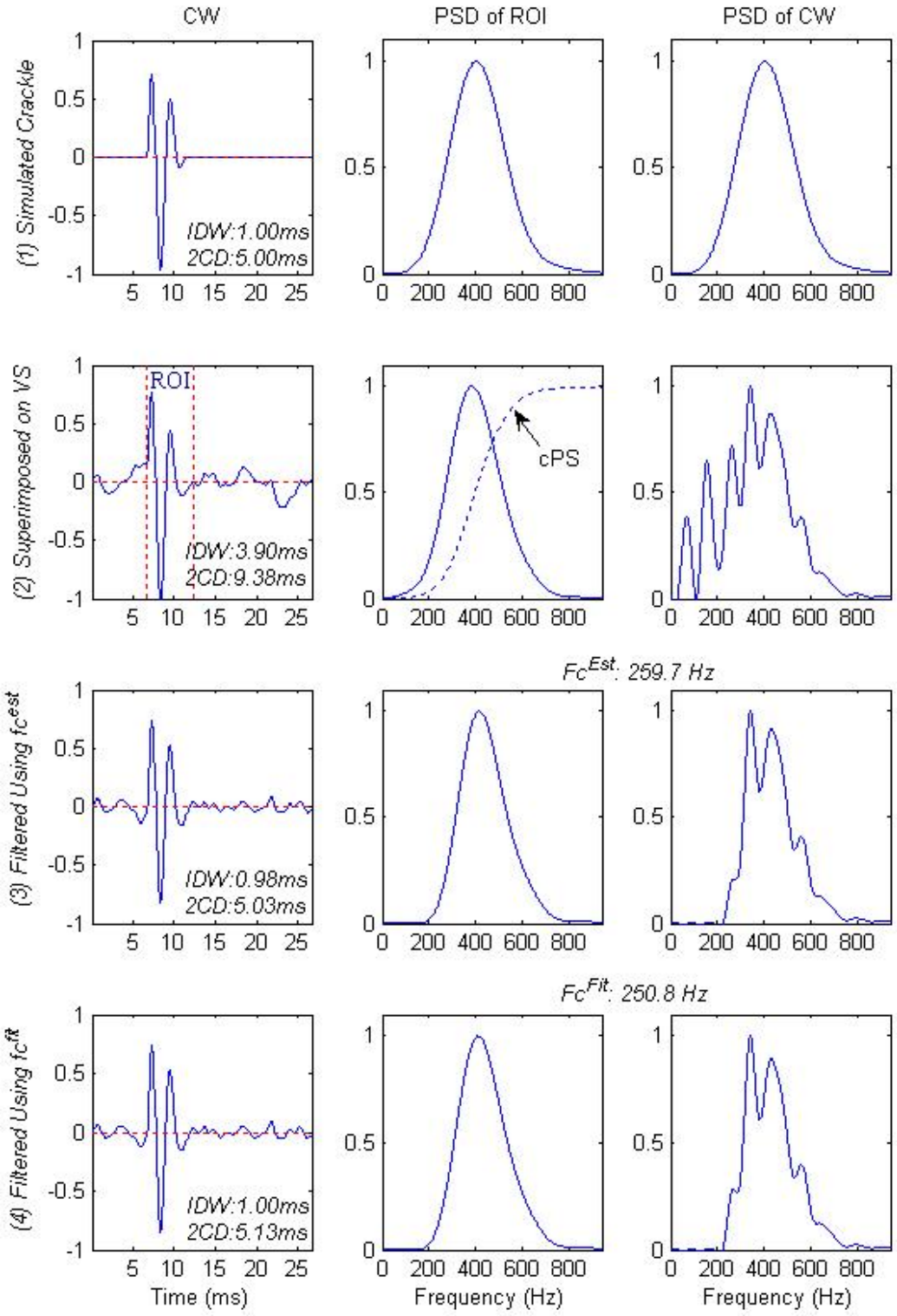

Figure 2.9 The waveforms and frequency spectra for a simulated fine crackle at each step of algorithm, i.e. (1) crackle simulation, (2) superimposition of the simulated crackle on VS window, filtering of the crackle using (3) f_c^{est} and (4) f_c^{fit}. The figures on the left for each class show the crackles in the time domain whereas those on the right show frequency responses of ROIs with respective cPSs and of CWs. The resulting crackle parameters are given on the figures of VS windows and f_c^{est} and f_c^{fit} on the figures of frequency responses.

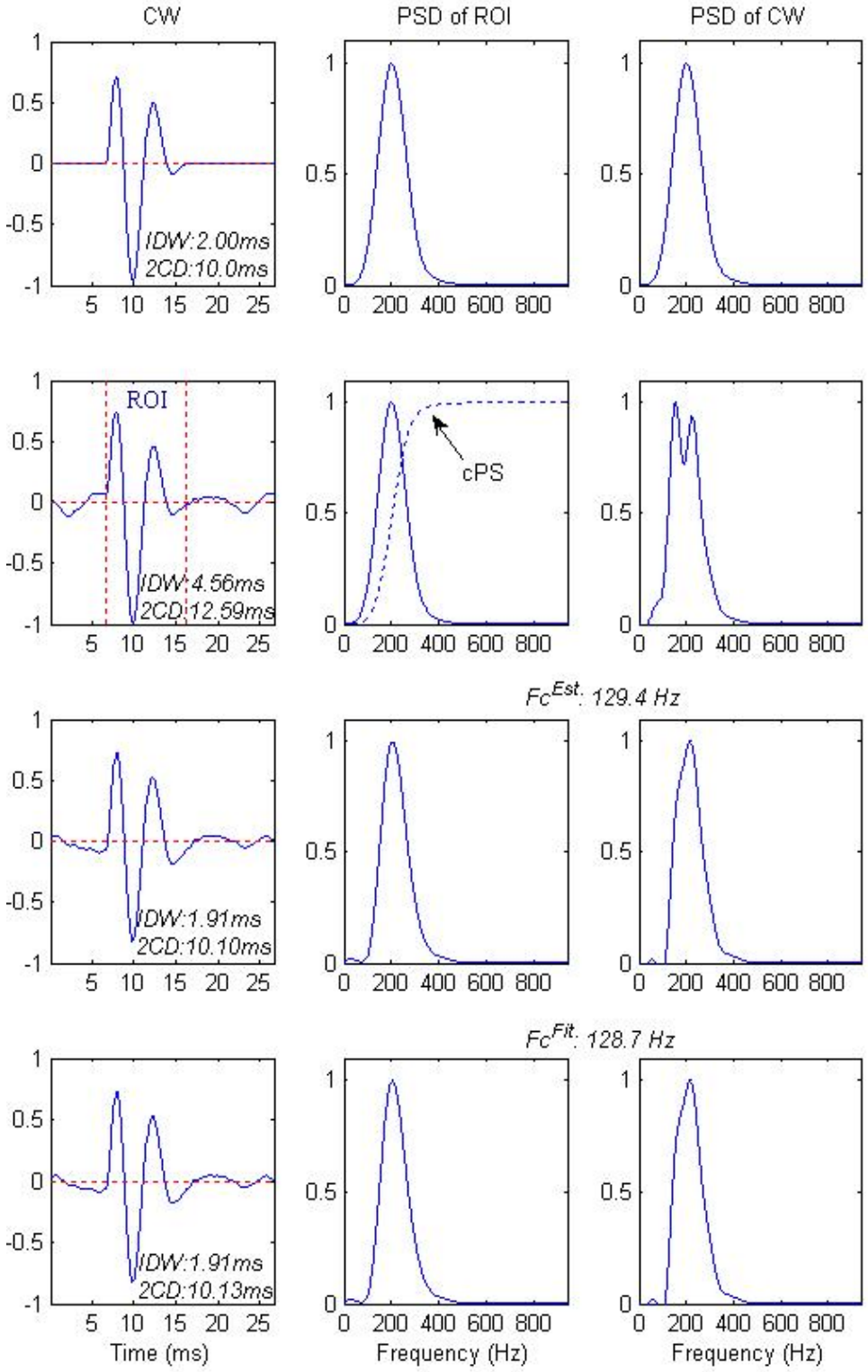

Figure 2.10 The waveforms and frequency spectra for a simulated coarse crackle at each step of algorithm.

Table 2.2
*AER*s for *FC*s according to *IDW* and 2*CD* through the VS elimination algorithm with respect to sub-phases, i.e. early, mid, late inspiration and expiration. The 1st row indicates *AER* after superimposing simulated *FC*s on *VSs*. The 2nd row shows *AER* after wavelet filtering (*WF*) by eliminating 6th wavelet component. The 3rd and 4th rows show *AER* after filtering using f_c^{est} and f_c^{fit}.

	IDW						2CD					
	Inspiration			Expiration			Inspiration			Expiration		
	Early	Mid	Late	Early	Mid	Late	Early	Mid	Late	Early	Mid	Late
Raw	94.9%	87.5%	99.2%	99.4%	92.7%	96.7%	51.6%	42.7%	54.8%	67.7%	66.1%	63.1%
WF	44.5%	44.9%	38.0%	42.7%	42.9%	38.0%	22.4%	21.7%	19.7%	21.8%	23.2%	20.0%
f_c^{est}	6.9%	6.0%	6.3%	8.5%	9.0%	7.8%	9.7%	9.0%	8.9%	11.6%	13.3%	10.7%
f_c^{fit}	8.6%	7.2%	8.4%	12.5%	12.0%	9.4%	10.4%	9.3%	9.1%	12.8%	13.7%	10.8%

Table 2.3
*AER*s for *CC*s according to *IDW* and 2*CD* through the VS elimination algorithm with respect to sub-phases of respiratory cycle.

	IDW						2CD					
	Inspiration			Expiration			Inspiration			Expiration		
	Early	Mid	Late	Early	Mid	Late	Early	Mid	Late	Early	Mid	Late
Raw	52.3%	45.9%	53.5%	56.8%	55.2%	58.1%	19.2%	17.0%	22.3%	26.8%	25.6%	26.1%
WF	12.2%	12.2%	12.1%	12.2%	12.3%	12.1%	14.0%	14.1%	14.0%	14.2%	14.1%	14.1%
f_c^{est}	5.4%	5.2%	5.7%	5.9%	6.2%	6.0%	6.3%	5.9%	6.8%	8.2%	7.9%	7.8%
f_c^{fit}	5.7%	5.3%	6.0%	6.6%	7.2%	7.6%	7.2%	6.6%	7.4%	8.8%	8.9%	8.6%

tortion due to background VS and those of filtered crackles. The mean distortion of crackle parameters due to *VSs* and the results of three filters are summarized in Tables 2.2, 2.3 and 2.4. In Table 2.2, mean value of the distortion amount of *FC* parameters in different subphases of the respiratory cycle is given whereas the results of the same evaluation for *CC*s are given in Table 2.3. In Table 2.4, the variations in parameters for *FC*s and *CC*s are summarized based on the inspiration and expiration, respectively. When simulated crackles are superimposed on VS, the resulting distortions for *IDW* for *FC*s and *CC*s are in the range 87.5%-99.4% (0.88ms-0.99ms) and 45.9%-58.1% (0.92ms-1.06ms), respectively whereas *AER*s of 2*CD* for *FC*s and *CC*s are in the range 42.7%-67.7% (2.14ms-3.39ms) and 17.0%-26.8% (1.70ms-2.68ms), respectively.

Table 2.4
Average AERs for FCs and CCs according to IDW and $2CD$ through the VS elimination algorithm with respect to semi-cycles, i.e. inspiration and expiration.

	FC				CC			
	IDW		2CD		IDW		2CD	
	Ins	Exp	Ins	Exp	Ins	Exp	Ins	Exp
Raw	94.0%	96.3%	49.9%	65.3%	50.7%	56.8%	19.6%	26.2%
WF	42.4%	40.8%	21.3%	21.5%	12.2%	12.2%	14.0%	14.1%
f_c^{est}	6.4%	8.4%	9.2%	11.7%	5.4%	6.0%	6.3%	8.0%
f_c^{fit}	8.1%	11.1%	9.6%	12.2%	5.7%	7.2%	7.1%	8.8%

Table 2.5
Processing times of calculating f_c^{est} and f_c^{fit} for a single crackle.

T^{est}	49.1 ±13.6ms
T^{fit}	5.30±0.96ms
T^{est}/T^{fit}	9.26

Wavelet filtering reduces this distortion to around 40% and 20% for IDW and $2CD$ of FCs, respectively. For CCs, the distortion after wavelet filtering reduces to 12% and 14% for IDW and $2CD$, respectively. In the proposed method, the overall performance is at least twice better than the wavelet filter. The inspiratory performance is higher than expiratory performance for both FCs and CCs. Although the variations change with different subphases of the respiration cycle, the mean error is less than 8.4% for filters with f_c^{est}. The variations in FCs are slightly greater that those of CCs. AERs for IDW and $2CD$ of FCs are in the range 6.0%-9.0% (0.06ms-0.09ms) and 7.8%-13.3% (0.39ms-0.67ms), respectively whereas AERs for IDW and $2CD$ of CCs are in the range 5.2%-6.2% (0.10ms-0.12ms) and 5.9%-8.2% (0.59ms-0.82ms), respectively.

As expected, when f_c^{fit} is used in filtering, the error rates increase slightly in the range by 0.3% - 2.7%. However when the reduction in computational cost is considered, the use of f_c^{fit} is justified especially in real-time analysis as the following analysis indicates. The processing times from calculating PSD of ROI to determination

of f_c for the two algorithms are given in Table 2.5.

As indicated in Table 2.5, using f_c^{fit} decreases computational time by almost ten-fold which is especially important for real-time applications where a large number of crackles is to be processed. After the verification on the simulated crackles, the proposed method is applied to real data set consisting of 2811 crackles recorded from 13 subjects with varying respiratory diseases. Two samples of recorded and filtered crackles with their corresponding PSDs are depicted in Figure 2.11 and 2.12.

In order to see the effect of filtering on the crackle parameters, crackles from one subject with pneumonia and one with COPD were used. Their scatter plots and histograms showing the ratio of IDW and $2CD$ before and after filtering are depicted in Figure 2.13. The changes of crackle parameters of real data including 2811 crackles after filtering with f_c^{est} and f_c^{fit} are depicted in Figure 2.14. The peaks of the histogram appear at 0.004 and -0.002 which correspond to the ratios of 1.010 and 0.996. In both histograms, the ratio of crackles with $2CD$ elongation to those with shortening due to VSs is two to one as expected. The range of change in parameters extends up to 10-fold for a small number of crackles.

High precision is necessary in determining f_c that eliminates the background VS. To investigate this requirement of precision, the sensitivity of crackle waveform to cut-off frequencies is demonstrated based on crackle parameters. Simulated FC and CC superimposed on one full respiratory cycle of VSs are used to measure the distortion of the waveform with respect to known reference values of crackle parameters.

f_c at which minimum AER is achieved is defined as optimum f_c (f_c^{opt}) for each experiment. To observe the effect of filtering using the neighbors of f_c^{opt} as fc, the frequencies within $\pm 25\%$ neighborhoods of f_c^{opt} are used as f_c and the mean of AERs are calculated for each neighbor percentage frequency. Separate simple linear regressions are performed on the mean AERs of the neighbor percentage frequencies for the lower and higher frequency range with respect to the f_c^{opt}. Plots of AERs of IDW and $2CD$ for both FCs and CCs with respect to percentage frequency are

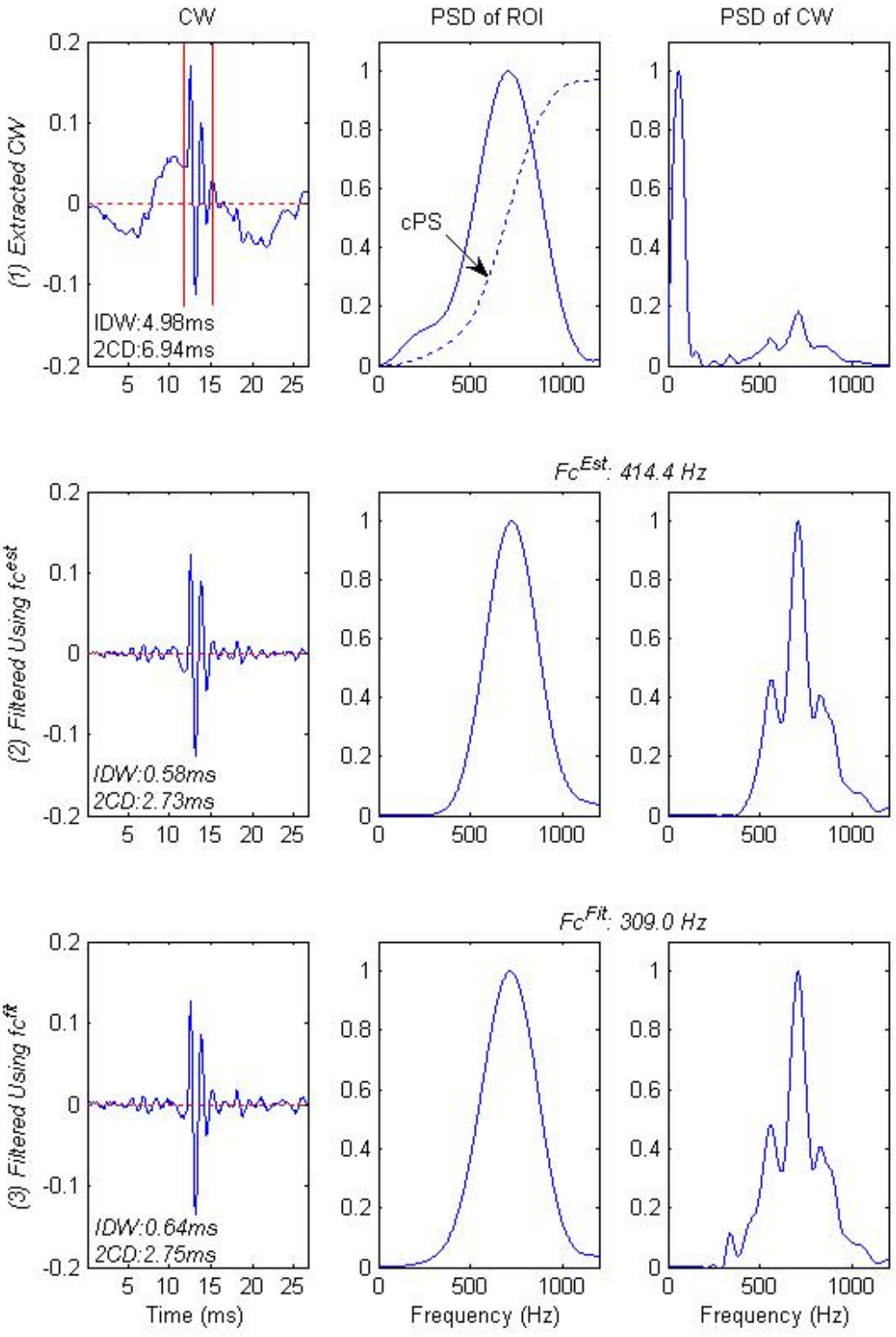

Figure 2.11 The procedure of VS elimination algorithm applied on a real fine crackle. The procedure has three steps: Extraction of CW and determining ROI (on the 1st row), and filtering using f_c^{est} (on the 2nd row) and f_c^{fit} (on the 3rd row). The first columns show the CWs whereas the second and third columns show PSDs of ROIs and CWs, respectively. The cPSs of raw crackles are depicted in the figures of PSD of ROI. The values of crackle parameters before and after filtering are indicated on the figures of CWs.

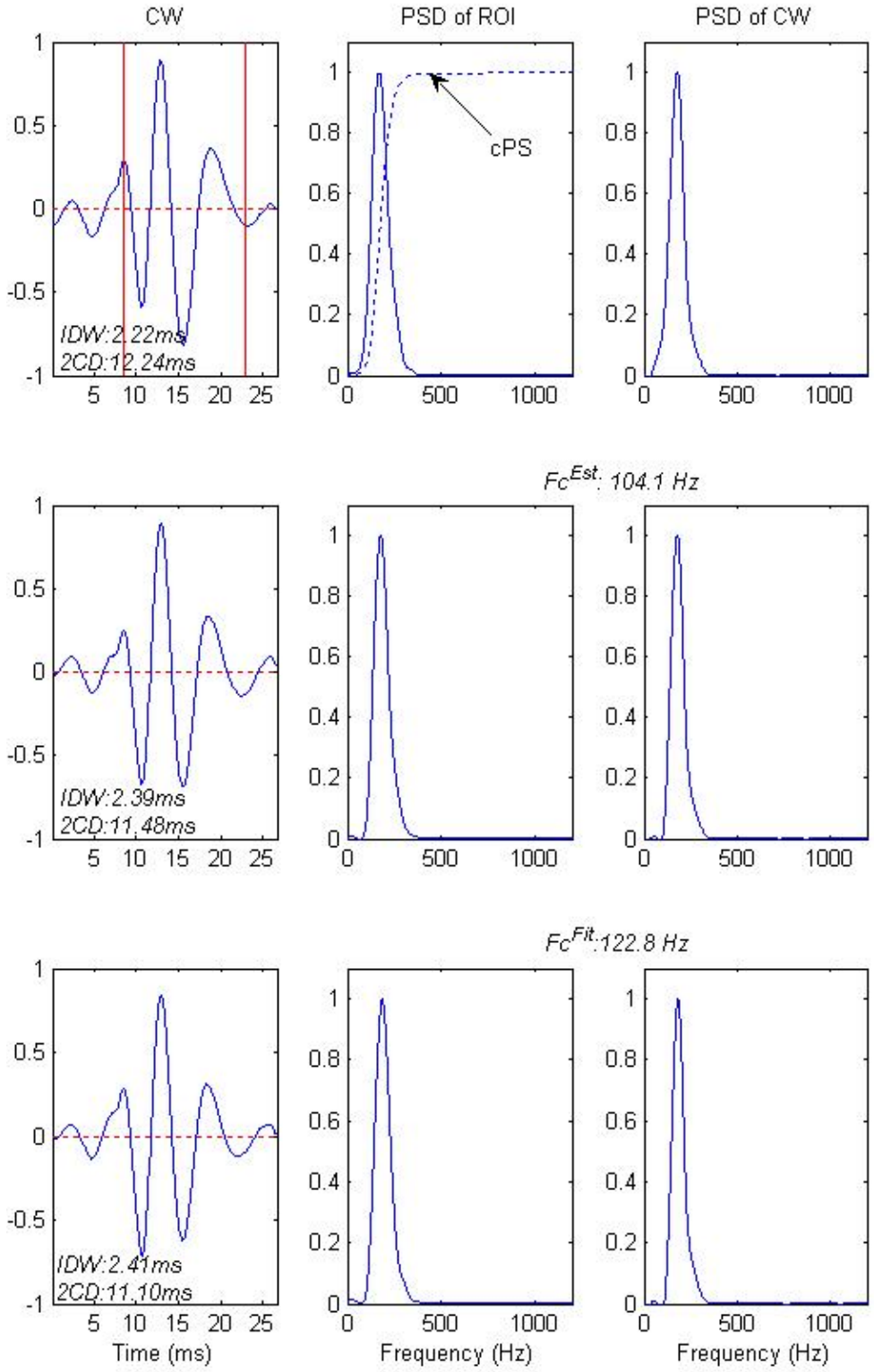

Figure 2.12 The procedure of VS elimination algorithm applied on a real coarse crackle.

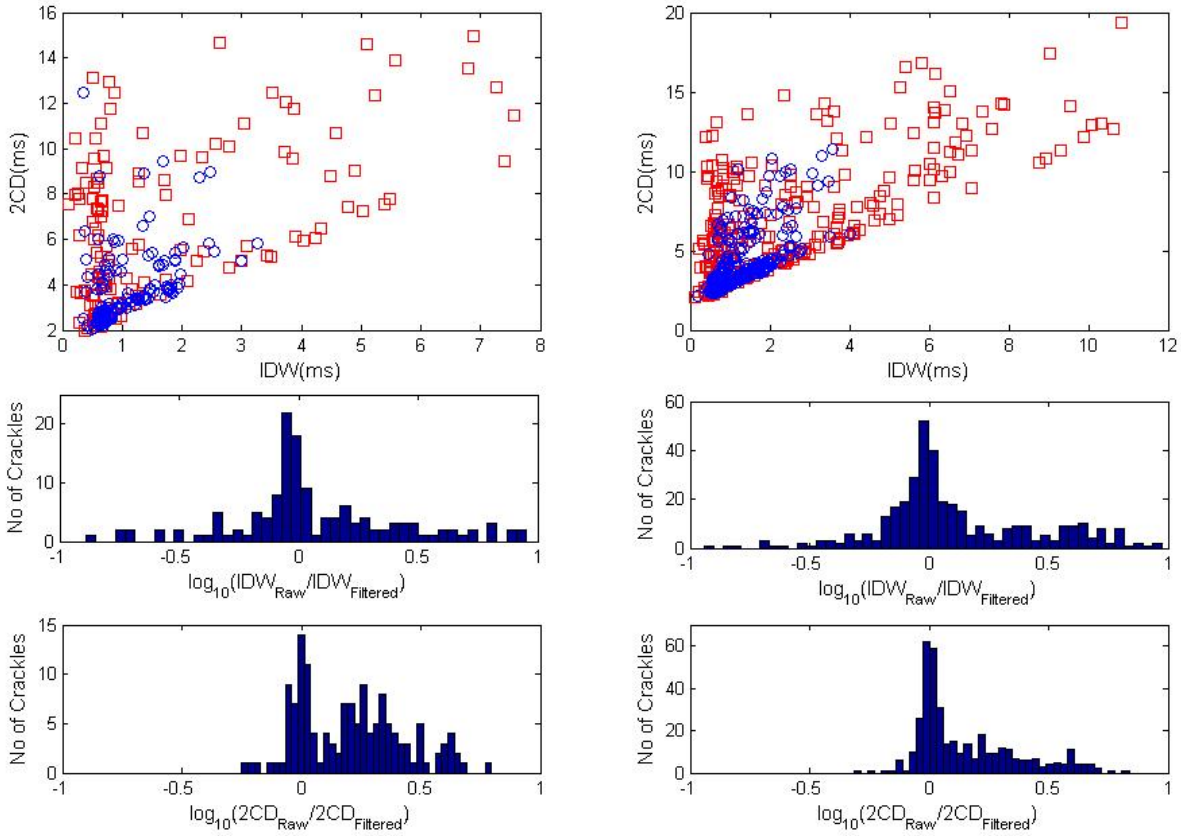

Figure 2.13 Crackle parameters belonging to two subjects with pneumonia (left) and COPD (right) before (red square) and after (blue circle) filtering using f_c^{est}. The histograms in the second and third figures show the ratios between raw and filtered parameters in logarithmic scale that indicate the variations in parameters via filtering.

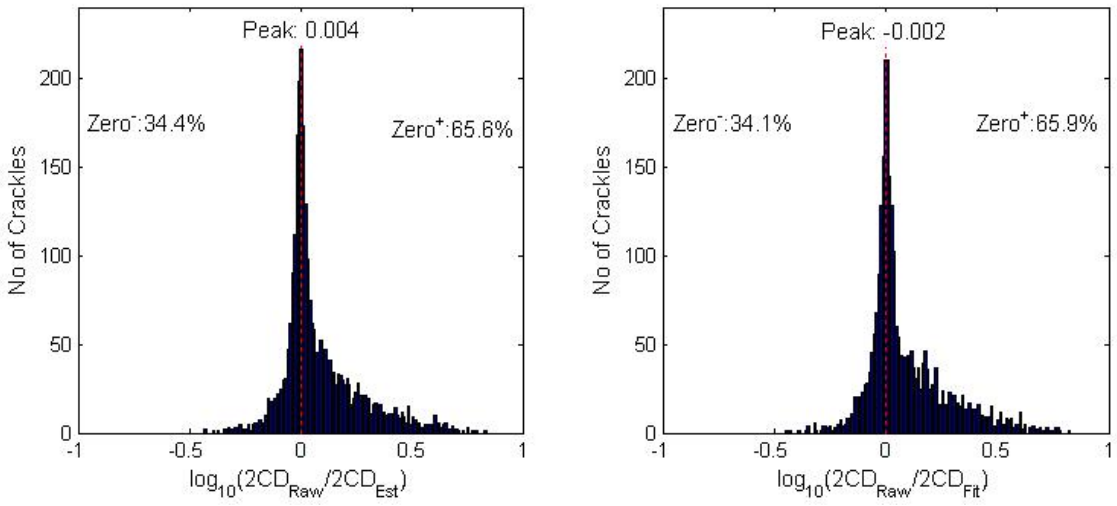

Figure 2.14 The ratios between raw and filtered crackle parameters using f_c^{est} (left) and f_c^{fit} (right) in a logarithmic scale. Zero- and Zero+ represent the ratios of negative and positive values, respectively and thus indicate whether raw crackle parameters are lower or higher than filtered crackle parameters.

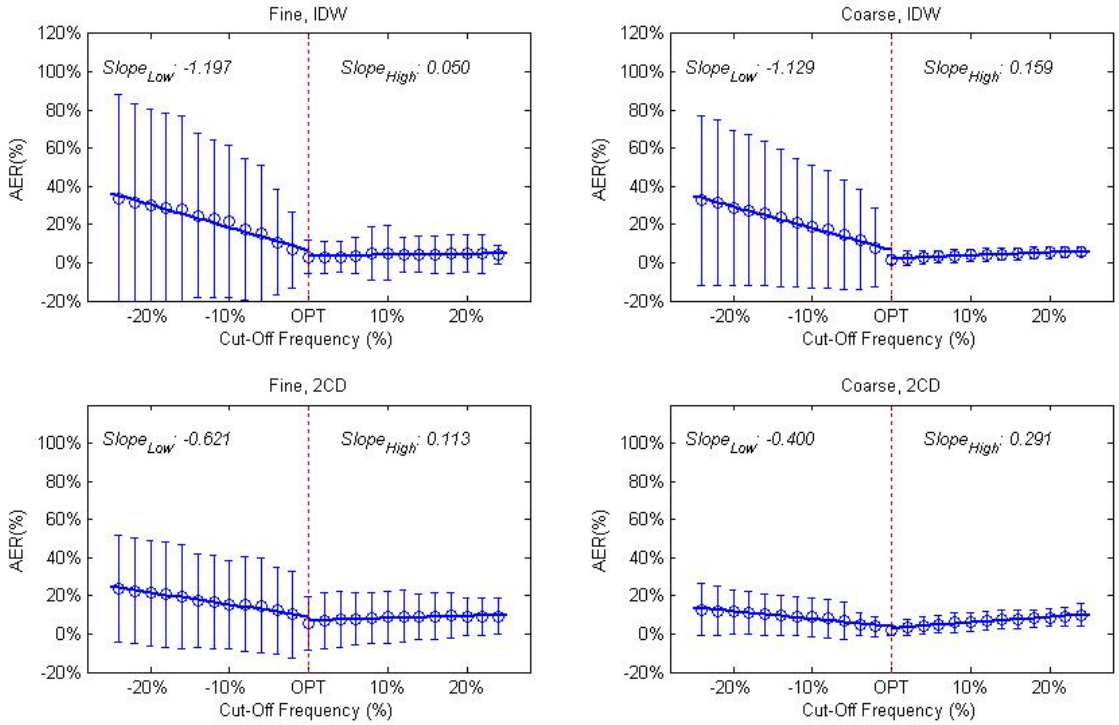

Figure 2.15 f_c sensitivities of crackle parameters.

depicted in Figure 2.15. The slopes of the linear curves represent the sensitivity of the crackle waveforms to lower and higher cut-off frequencies since sensitivity is defined as AER change per percentile of f_c^{opt}.

The f_c^{opt} represents the f_c at which the elimination of VS is performed with highest success therefore the slope for lower frequencies demonstrates the behavior of parameters until optimum elimination of the VSs is achieved. Thus it can be stated that the errors depict the effect of presence of VS. The slope for higher frequencies demonstrates the behavior of parameters after the elimination of the VSs therefore the error stems from the waveform distortion based on filtering out of crackle components.

Table 2.6 summarizes the sensitivities of both IDW and $2CD$ for FCs and CCs for frequencies lower and higher than f_c^{opt}. For lower frequencies, IDW and $2CD$ sensitivities of FCs are 1.197 and 0.621 (11.97 $\mu s/pof$ and 31.05 $\mu s/pof$), respectively, whereas those of CCs are 1.129 and 0.400 (22.58 $\mu s/pof$ and 40.00 $\mu s/pof$) respectively. "pof" stands for percentile of f_c^{opt}. IDW represents higher-pitch components

Table 2.6
f_c sensitivities of crackle waveforms for lower (LF) and higher (HF) frequencies according to AER and corresponding error in time.

		LF		HF	
		AER	µs	AER	µs
Fine	IDW	1.197	11.97	0.050	0.50
	2CD	0.621	31.05	0.113	5.65
Coarse	IDW	1.129	22.58	0.159	3.18
	2CD	0.400	40.00	0.291	29.10

of crackles and is proportionally more affected by VSs since its duration is smaller than $2CD$. Therefore, as expected, IDW sensitivity is higher than $2CD$ sensitivity for lower frequencies. On the other hand, $2CD$ sensitivity is higher than IDW sensitivity for higher frequencies since $2CD$ represents lower -pitch components of crackles. The sensitivity figures for IDW and $2CD$ of FCs are 0.050 and 0.113 (0.50 $\mu s/pof$ and 5.65 $\mu s/pof$), respectively, whereas those for CCs are 0.159 and 0.291 (3.18 $\mu s/pof$ and 29.10 $\mu s/pof$), respectively.

Sensitivities for higher frequencies for both parameters and for both crackle types are lower than sensitivities for lower frequencies since the distortions at lower frequencies stem from VSs whereas losing some frequency components of the crackle waveform causes the distortion at higher frequencies.

As the analysis shows, the crackle parameters are very sensitive to f_c and if correct values of parameters are to be extracted from crackle waveform, the design of the filter for removing VS should be carried out with maximum care.

3. MODELING OF PULMONARY CRACKLES USING WAVELET NETWORK

In this chapter, the aim of the study is to automatically depict the crackle waveform with only a small set of meaningful parameter values as is necessary for typical discrimination tasks and to this end, WNs have been employed. WNs can be used as signal modeling tools and are based on a specific network structure where the nodes are described by wavelet functions [76, 25, 14, 24, 12, 28]. They are especially useful in representing nonstationary, time-varying signals. Wavelet functions have been utilized in the studies related to pulmonary crackles, particularly in detecting these nonstationary signals within the background of VSs [57, 23, 52, 1, 30, 73, 63, 29]. In this study, however, wavelet functions, namely complex Morlet wavelet, are used at the nodes of a network to model the crackle and thus obtain parameters from that model that are relevant to the pulmonary sound research. Single-node and double-node networks have been employed on a dataset of pulmonary crackles from a wide range of frequency spectrum with the double node modeling rendering smaller modeling error. The model is shown to represent the morphology of the crackle waveform with five parameters per node. The parameters extracted from the WN models have been used along with the traditional parameters in a two-class clustering experiment with a view to compare the correspondence between diverse crackle parameter sets and crackle types.

3.1 Methodology

3.1.1 Wavelet Network Modeling

A WN used for modeling has a neural network structure that performs wavelet functions as transfer functions in their hidden nodes instead of sigmoid functions that are employed in conventional multi-layer perceptrons (MLP). A wavelet, in definition,

has a finite energy that is concentrated in a time interval [10]. Therefore, fewer nodes are used in the interpretation of transient signals with WN as compared to MLP [75], in a similar manner of radial basis functions that use Gaussian functions as transfer functions. Moreover, the wavelet function can be selected according to the characteristics of target signals to reduce the number of nodes in signal interpretation. In our application, the cM wavelet function is employed to model the pulmonary crackles due to both the similarities between the waveforms of the crackles and the cM function and the flexibility of the cM function in the modeling process. The cM function ($h(t)$) is defined as

$$h(t) = exp(-t^2/2 + j\omega_0 t) \tag{3.1}$$

where ω_0 is a constant of modulating frequency that equals to 5.33. To improve the estimation of the target signal with smaller number of nodes, the modulating frequency ((ω)) is not employed as a constant but rather as a variable.

The employed wavelet network having a single-hidden-layer structure with K-nodes is depicted in Figure 3.1. The estimated signal ($\hat{x}(t)$) in the output node is the weighted summation of the wavelet functions in the hidden nodes and is interpreted as

$$\hat{x}(t) = \sum_{k=1}^{K} w_k h(\frac{t - b_k}{a_k}) \tag{3.2}$$

where w_k is a weight factor and $h(.)$ is the wavelet function with scaling (a_k) and time shifting (b_k) parameters for the k^{th}-node. Substituting the cM function into Eq. 3.2 and converting it into the real notation, the estimated signal is interpreted as

$$\hat{x}(t) = \sum_{k=1}^{K} \left[w_{\cos,k} \cos(\omega_k \frac{t - b_k}{a_k}) + w_{\sin,k} \sin(\omega_k \frac{t - b_k}{a_k}) \right] \exp\left(-0.5(\frac{t - b_k}{a_k})^2 \right) \tag{3.3}$$

where $w_{\cos,k}$ and $w_{\sin,k}$ are the weight factors of cosine and sine terms of the k^{th}-node, respectively. Thus, the contribution of each node to the output node is the weighted sum of sine and cosine terms that are windowed by the exponential function, i.e. the Gaussian window. b_k and a_k^2 are the center and the variance of the Gaussian window, respectively, whereas ω_k and a_k are the parameters related to the spectral components

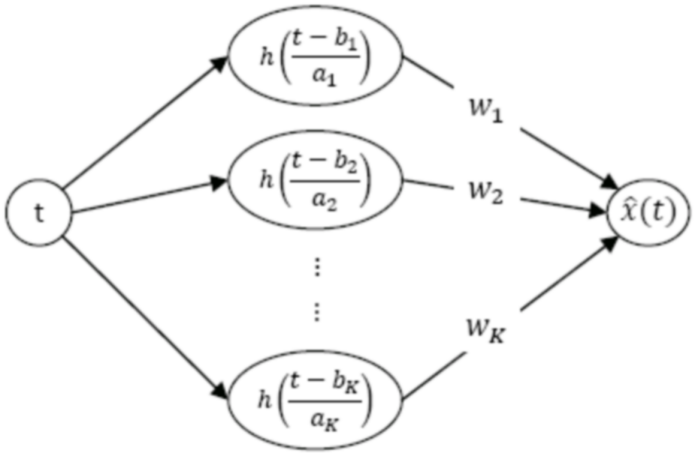

Figure 3.1 The structure of wavelet network with single hidden layer

of the output signal. Moreover, $w_{\cos,k}$ and $w_{\sin,k}$ correlate with the ratios of deflection amplitudes therefore the morphology of the signal. Note that the cosine portion of the signal is in phase whereas the sine portion is $\pi/2$ degrees out of phase with the Gaussian window.

In the modeling process, the modeling error (ε) for an N-sample target signal ($x(t)$) is defined with the least square point of view as

$$\varepsilon = \sum_{i=1}^{N} [x(t_i) - \hat{x}(t_i)]^2 \tag{3.4}$$

Learning rules in the iterative process of modeling are defined on the partial derivatives of the error with respect to the five variables, i.e. $\partial\varepsilon/\partial a_k$, $\partial\varepsilon/\partial b_k$, $\partial\varepsilon/\partial\omega_k$, $\partial\varepsilon/\partial w_{\cos,k}$ and $\partial\varepsilon/\partial w_{\sin,k}$ that are described as following formulas in the study of Dickhaus et al. [2]. Instead of $\partial L/\partial a_k$, the partial derivatives $\partial L/\partial a_k^{-1}$ are preferred in the modeling in order to reduce the complexity of the calculation and, therefore, the computational cost.

$$\frac{\partial\varepsilon}{\partial w_{cos,k}} = -\sum_{i=1}^{N} R.C.E \tag{3.5}$$

$$\frac{\partial\varepsilon}{\partial w_{sin,k}} = -\sum_{i=1}^{N} R.S.E \tag{3.6}$$

$$\frac{\partial \varepsilon}{\partial a_k^{-1}} = -\sum_{i=1}^{N} \left[R.E.(t_i - b_k)\left(-w_{cos,k}(F.C - \omega_k.S) - w_{sin,k}(F.S + \omega_k.C)\right)\right] \tag{3.7}$$

$$\frac{\partial \varepsilon}{\partial b_k} = -\sum_{i=1}^{N} \left[R.E.\frac{1}{a_k}\left(w_{cos,k}(F.C + \omega_k.S) + w_{sin,k}(F.S - \omega_k.C)\right)\right] \tag{3.8}$$

$$\frac{\partial \varepsilon}{\partial \omega_k} = -\sum_{i=1}^{N} \left[R.E.F.(-w_{\cos,k}.S + w_{\sin,k}.C)\right] \tag{3.9}$$

where $C = \cos(\omega_k \frac{t-b_k}{a_k})$, $S = \sin(\omega_k \frac{t-b_k}{a_k})$, $E = \exp\left(-0.5(\frac{t_i-b_k}{a_k})^2\right)$, $R = x(t_i) - \hat{x}(t_i)$, and $F = \frac{t_i-b_k}{a_k}$.

In trying to minimize the modeling error, different initial points are selected in the space of a_k and ω_k to overcome the local minima problem. The initial value for b_k is selected as the midpoint of the target signal whereas $w_{\cos,k}$ and $w_{\sin,k}$ are initialized as zero.

3.1.2 Model-based Clustering

The consistency between the WN parameters and the conventional parameters of crackles is analyzed according to the distribution and localization of crackles in the respective parameter spaces of WN and conventional methods. The crackles are generally categorized into two groups, i.e. fine and coarse, however there is no golden standard to discriminate the two groups. Therefore, the classification analysis of crackles is performed in an unsupervised manner and the percentage of true-matching of labeling according to conventional and WN parameters are then calculated. In this clustering analysis, it is assumed that the data is a multivariate normal mixture, and therefore the crackles distribute according to the probability densities of their groups [4, 18]. The expectation maximization algorithm [13] based on the maximization of the data likelihood is performed to differentiate the crackle groups and thus determine the crackle labels. The details are described in the next chapter.

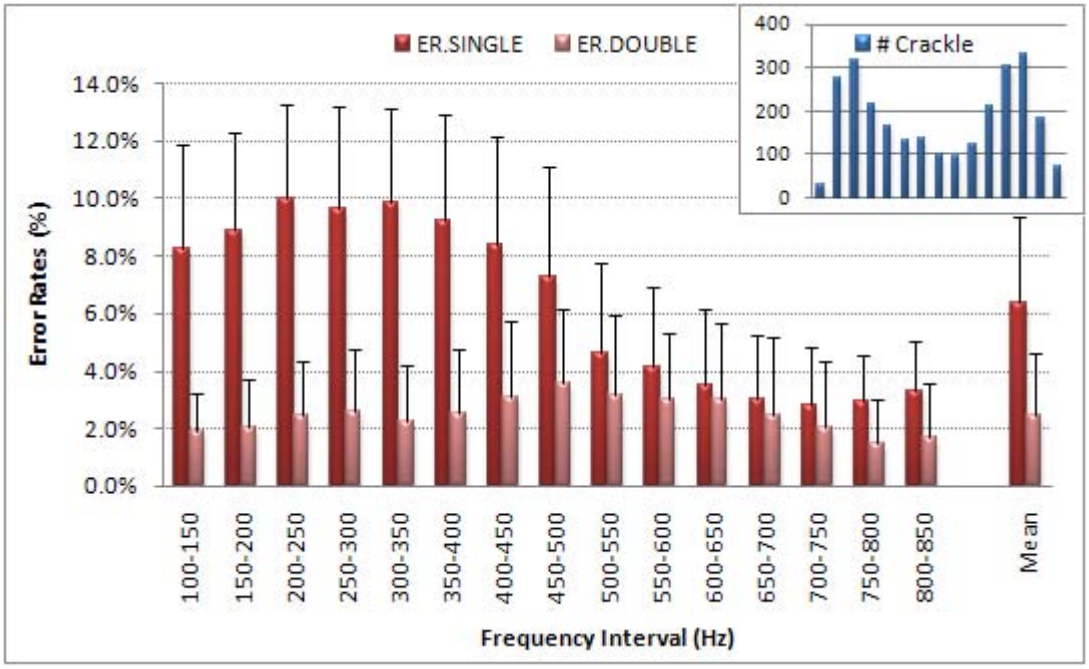

Figure 3.2 Error rates of crackle modeling using single- and double-node WN according to median frequencies of crackles. The small figure at the upper-right corner shows the number of crackles at the corresponding frequency interval.

3.2 Results

Since conventional crackle parameters are defined on the first two cycles (2CD) of the crackle waveform, modeling with WNs is also performed on this region. WNs with single-node engage the node to interpret two cycles together whereas the two nodes in the double-node WN model the first and second cycles separately. Therefore, the expanding waveform of the crackle can be represented by double-node WN with lower modeling error whereas single-node WN represents peak frequency component of crackle since the learning rules work iteratively to reduce the square of the error. However, the computational cost of modeling with double-node WN is approximately twice that of single node WN.

Error rate (ER) is defined as the ratio between the energies of residual (error) signal and target signal and is calculated for the N-sample target signal as

$$ER = \frac{\sum_i^N (x_i - \hat{x}_i)^2}{\sum_i^N x_i^2}.100\% \tag{3.10}$$

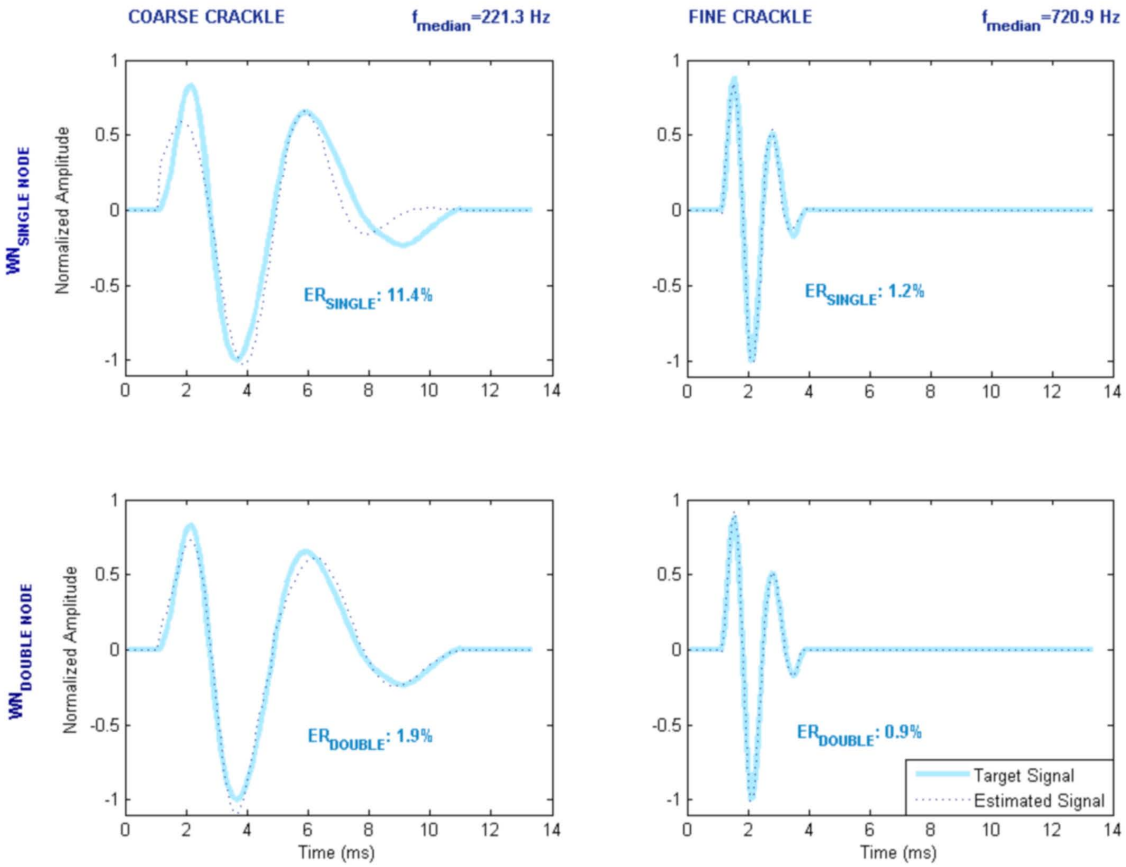

Figure 3.3 The waveforms of target (solid line) and estimated (dotted line) signals. One sample from each coarse and fine crackle having the median frequency between 200-250Hz and 700-750Hz frequency band is selected. The signals estimated using single- and double-node WN are shown in the first and second rows, respectively.

The ERs categorized according to the spectral components of crackles are depicted in Figure 3.2 to observe the performance of modeling using single- and double-node WN with a view to emphasize the performance difference of modeling between that of coarse and fine crackles. In the figure, ERs are grouped according to the median frequency of cumulative power spectrum of crackles. The median frequency of cPS corresponds to 50% of the total energy.

The performances of double-node WN lie in the band of 1.5-3.6% error rate whereas the error rates of single-node WN range from 2.8% to 10.0%. The average error rates for single- and double- nodes are approximately 6.5% and 2.5%, respectively. The difference between average performances of single- and double-node WNs stems mainly from high error rates of single-node WN for modeling crackles with low median

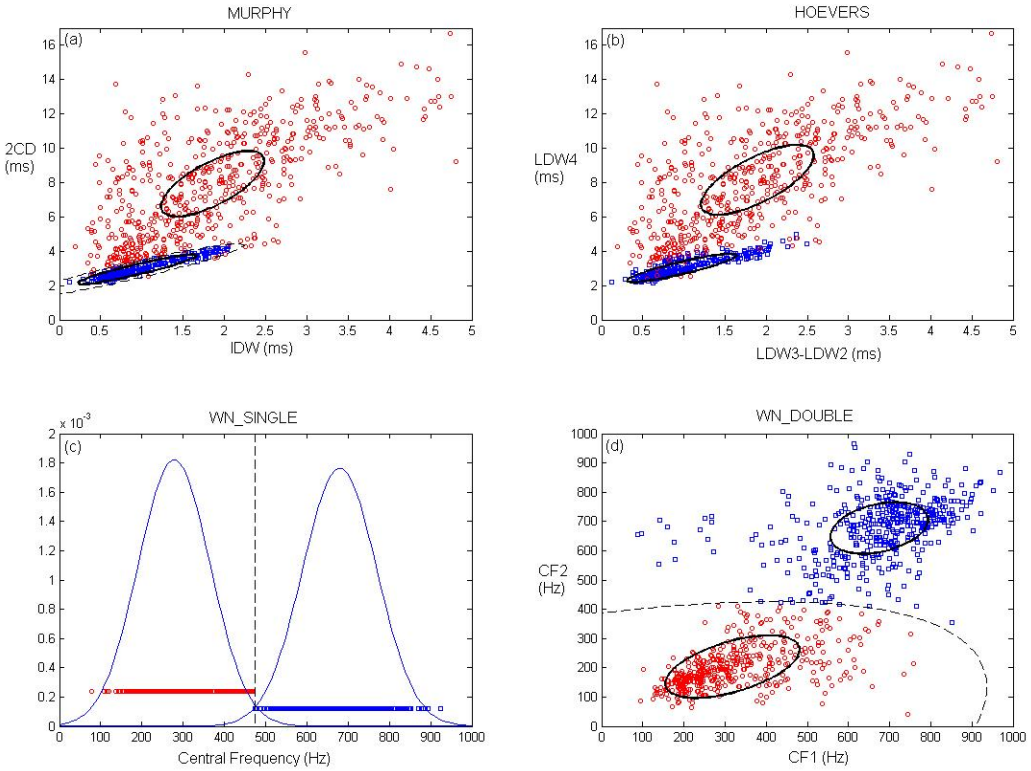

Figure 3.4 Clustering of crackle samples according to the four feature sets, i.e. Murphy, Hoevers, single and double-node WN. The ellipses represent the covariances of two-multivariate clusters, i.e. fine and coarse in (a), (b) and (d). The curves in (c) represent the likelihood of the two clusters. The dashed lines are the discriminants between the clusters that separate the feature spaces into fine and coarse subspaces. (b) For comparative observation of separation of spaces using Hoevers with Murphy feature sets, the four features of Hoevers are projected into two features that correspond to the IDW and $2CD$. In scatter plots, one third of samples are shown to reduce ink-to-noise ratio.

frequency, corresponding to coarse crackles. The reason for this lower performance is illustrated in Figure 3.3 where the performances of single and double-node WN on one fine and one coarse crackle with median frequencies in the range of 200-250Hz and 700-750Hz, respectively, are observed, pointing to the relatively high ER in modeling a coarse crackle with a single node WN, namely, 11.4% ER as opposed to 1.9% ER of a double node WN. The corresponding ERs for a fine crackle, on the other hand, are 1.2% and 0.9%, respectively. In other words, crackles with coarse spectral components have proportionally more expanding waveforms than fine crackles. Since each node of WN has monophonic transfer function and the modeling error optimization is made in the least square sense, single-node WN represents the spectral component of the target signal with peak energy.

To observe the consistency between conventional parameterization methods and

Table 3.1
Confusion matrices for clustering analysis of fine and coarse crackles using four feature sets. The confusion matrices on the diagonal of the table shows the numbers of samples labeled as fine and coarse crackles. The right off-diagonal elements of the tables are the confusion matrices that show the true and false matching of labeling according to different feature sets. The left off-diagonal elements of the table are the accuracies of labeling that is defined as the ratios of true-matching to the total number of crackles. (F: Fine and C: Coarse)

		Murphy		Hoevers		WN.Single		WN.Double	
		F	C	F	C	F	C	F	C
Murphy	F	997		978	19	992	5	996	1
	C		1714	118	1596	448	1266	324	1390
Hoevers	F	*95.0%*		1096		1095	1	1096	0
	C				1615	345	1270	224	1391
WN.Single	F	*83.3%*		*87.2%*		1440		1289	151
	C						1271	31	1240
WN.Double	F	*88.0%*		*91.7%*		*93.3%*		1320	
	C								1391

WN in representing crackle type, distribution of crackle parameters in feature spaces are analyzed using model-based clustering as described in the methodology section. If there is a consistency between the two feature sets that are constructed using different parameterization methods, a crackle will belong to the same cluster, irrespective of which feature set is used.

Figure 3.4 shows the distribution of crackle samples in the different feature spaces and the separation of the feature spaces into two subspaces for fine and coarse crackles. The dashed lines show the boundaries between the two crackle groups. The expanding nature of the crackle waveforms with decreasing median frequency which accounts for the higher error rate for single WN modeling can further be depicted in Fig. 5d where the distribution of the central frequencies of the first and second cycles of the crackle as obtained from double node WN modeling is shown. The means of central frequencies of the first and second cycles of the coarse cluster are approximately 300Hz and 200Hz, respectively whereas those of both cycles of the fine cluster are approximately 700Hz.

Table 3.1 shows the true-matching of labeling according to clustering analysis shown in Figure 3.4. The diagonal elements of the confusion matrices are the numbers of the true-matched crackles whereas the off-diagonal elements are the false-matched according to the corresponding two feature sets. For instance, 1391 of 1615 coarse labeled crackles of Hoevers are true-matched whereas 224 of 1615 crackles are labeled as fine using double-node WN.

The left off-diagonal elements of the table represent the percentages of clustering analysis matching accuracies using different feature sets. The matching accuracy calculated using the elements of confusion matrices is defined as the ratio of the summation of diagonal elements of confusion matrices to the total number of elements. It is observed that the matching accuracies between single-node WN and conventional parameters are lower than those of double-node WN due to the loss of information in modeling using single-node WN. It should be noted that the parameters of the two conventional methods are linearly dependent.

4. MODEL-BASED CLUSTERING OF PULMONARY CRACKLES

The objective of this chapter is to probe the existence of a third crackle type, medium, besides the traditionally accepted types, namely, fine and coarse crackles and, furthermore, to explore the representative parameter values for each crackle type. A set of clustering experiments have been conducted on pulmonary crackles to this end. A model-based clustering algorithm, the EM algorithm, is used and the resulting cluster numbers are validated with BIC. The raw crackle data are preprocessed using the algorithm which has been described in detail in Chapter 2. Five different feature sets are extracted from the preprocessed crackle samples, two of which are conventional parameters derived from the zero-crossings of crackle waveforms. The third feature set corresponds to the spectral components of the crackles whereas the remaining two sets are derived from a single- and double-node WN modeling. The results of the clustering experiments demonstrate strong evidence for the existence of a third crackle type. Moreover, the labels yielded by clustering experiments using different feature sets match for roughly 80% or more of the crackle samples, resulting in similar representative crackle parameter values of the three clusters for all feature sets.

4.1 Methodology

4.1.1 Feature extraction

Feature sets are constructed based on zero-crossings and frequency spectra of crackle waveforms. Since conventional parameters are defined on the first two cycles of crackle waveform, all feature sets are extracted from this part of the waveform for standardization. For selecting the region of interest of the crackle waveforms from pulmonary sound data, the peak of LDW_1 is used as a reference point to overcome the difficulty in the determination of the exact beginning of crackle waveform on VS signal

[26]. The features employed in this study correlate closely with auditory perception used in auscultation, which senses frequency components [15].

The feature sets can be categorized into two groups according to time domain and frequency domain. The first group consists of the two conventional feature sets defined on zero-crossings. Murphy's two parameters, i.e. IDW and $2CD$, constitute the first feature set whereas the second one consists of Hoevers' four parameters, LDW_{1-4}. The relationship between the two sets is described as

$$IDW = LDW_3 - LDW_2 \; and \; 2CD = LDW_4 \tag{4.1}$$

It is clear that the first feature set is linearly dependent on the second feature set.

The third feature set is extracted from the spectral components of the crackles and comprise of lower and upper quartile frequencies of cPS. cPS is defined as normalized cumulative summation of PSD that is estimated for N-length time array using the periodogram method as shown in Eq. 2.8. Normalized cPS indicates the fractional energy contained up to a certain frequency whereas PSD indicates the power of the signal at a particular frequency. The lower and upper quartile frequencies of cPS correspond to 25% and 75% of total energies.

The features in the fourth and fifth sets are extracted from the model parameters of crackles using WNs with a single and double node, respectively [73]. WNs have a neural network structure that performs wavelets as transfer functions in their nodes as described in the previous chapter. The wavelet functions achieve localization on a space using a single node in the like manner as Gaussian functions used in radial basis functions. Moreover, a proper wavelet function resembling the target waveform can be selected from wavelet families to achieve modeling with fewer nodes in the network structures. In this study, cM wavelet function is preferred to model crackles due to both the similarities between the waveforms of a crackle and the real part of cM and the flexibility of the Morlet function in modeling. The total number of parameters from each node is five, i.e. scaling (a_k), time-shifting (b_k), modulating frequency (ω_k), and

weight factors of cosine and sine parts. For the clustering analysis, only the frequency-based parameters, i.e. a_k and ω_k, are employed to obtain the crackle clustering results that can both interpret the auditory perception and be comparable with the other feature sets. The weight factors of cosine and sine include additional information, e.g. the ratios of deflection magnitudes, and this redundant information may scramble the clusters, thus, the weight factors are excluded from the feature set. Moreover, the time-shifting parameter does not bear any information correlated with the type of the crackle, therefore it is not used in the clustering algorithm, as well. Finally, a single parameter, i.e. central frequency (CF), is employed from each node k which combines two parameters and is calculated using a_k and ω_k as

$$CF_k = \omega_k / 2\pi a_k \tag{4.2}$$

Since the targeted crackle waveform consists of only two cycles, up to two hidden nodes are adequate to model the waveform. The CF calculated using single node interprets the common CF of crackle waveform whereas using double nodes offers to model the progressively wider waveform of crackles with a lower error. Each node is employed on one cycle of crackle waveform therefore the CFs of the first and second cycles can be calculated and the widening of the waveform based on the CFs can be observed.

4.1.2 Clustering Method

The analysis of the sample distribution in the feature space is made according to the probabilistic approach. In this case, it is assumed that the data may be interpreted with a multivariate probabilistic mixture model and the members of the clusters distribute according to the density function of their own cluster model. Therefore, the analysis is reduced to a problem of looking for the parameters of the density functions. However, since there is a lack of information about which cluster the samples belong to, the parameters cannot be calculated directly. The labels of the samples and the parameters of the density functions are estimated by maximizing the likelihood of the

samples that is defined for N samples and G clusters as

$$\ell(\theta|x_1, x_2, \ldots, x_N) = \prod_{1}^{N} \sum_{1}^{G} \tau_k p(x_i|\theta_k) \tag{4.3}$$

where $p(x_i|\theta_k)$ and θ_k are probability density and parameters of k^{th} cluster (C_k), respectively whereas τ_k is the prior probability that a sample belongs to C_k.

EM algorithm [13] is a commonly-used method to estimate the maximum likelihood of the samples that are considered to be composed of observed (x_i) and unobserved (z_i) variables. In our problem, the features acquired from crackles and the labels of the crackles are observed and unobserved variables, respectively. *EM* algorithm consists of iterative calculation of two steps. In the E-step, the expected value of the likelihood of the samples is computed according to the observed values and current model parameters. The yield of this step is the estimated labels of samples. In the M-step, the model parameters that maximize the expected value of the likelihood are estimated. If it is assumed that clusters have multivariate Gaussian distributions, in the E-step, the labels will be estimated as

$$\hat{z}_{ik} \leftarrow \frac{\tau_k |S_k|^{-1/2} exp[-(1/2)(x_i - m_k)^T S_k^{-1}(x_i - m_k)]}{\sum_{j=1}^{G} \tau_j |S_j|^{-1/2} exp[-(1/2)(x_i - m_j)^T S_k^{-1}(x_i - m_j)]} \tag{4.4}$$

where m_k and S_k are the mean and the covariance matrix of C_k, respectively. Although z_{ik} gets the value of 1 if x_i belongs to C_k and 0 if not, $\hat{z}_{ik}$ equals to the posterior probability that x_i belongs to C_k and can get values between 0 and 1 [4]. In the M-step, the estimated values of the parameters for normal mixtures are calculated as

$$m_k \leftarrow \sum_i \hat{z}_{ik} x_i / \sum_i z_{ik} x_i \tag{4.5}$$

$$S_k \leftarrow \frac{\sum_i \hat{z}_{ik}(x_i - m_k)(x_i - m_k)^T}{\sum_i \hat{z}_{ik}} \tag{4.6}$$

$$\tau_k \leftarrow (1/N) \sum_i \hat{z}_{ik} \tag{4.7}$$

The distributions of the clusters can be considered to be either spherical or nonspherical in shape and/or equal or unequal in size depending on the application [18]. Making a preference such as assuming spherical cluster distributions of equal size would reduce the number of parameters of covariance matrices and consequently convergence time, however the limitations on the cluster distributions may degrade the performance of the clusterer especially in the case of dissimilar cluster distributions. Therefore, constraining assumptions are not made on the covariance matrices of clusters to allow maximal flexibility in model distributions.

The unconstrained covariance matrices have $G(d(d+1)/2)$ independent variables for d-dimensional data, hence the convergence time of the algorithm is high. Therefore, a simpler method that yields appropriate initial values for the EM algorithm, which is sensitive to the initial values, is performed before EM. K-means algorithm is a partitioning algorithm which works according to the reconstruction error that is defined on the distances of the members of clusters to the means of their own clusters. From k-means to EM algorithm, the shapes of clusters change from spherical form to elliptic form. It should be noted that k-means algorithm is equivalent to the EM algorithm if the covariance matrices of the clusters are equal and proportional to the identity matrix [11]. Therefore, using k-means before EM, some spheres are placed on the distribution of the samples with lower performance and lower computational time and then the spheres are stretched to elliptical form for higher performance. In other words, the coarse work is initially done by the k-means whereas the fine work is performed by the EM algorithm. Since k-means algorithm is also sensitive to the initial values, the operation is replicated ten times and then the solution with minimum reconstruction error is used as initial values in the EM algorithm.

The optimum number of clusters (G_{opt}) is determined after estimating the cluster parameters for the values of G, $1, 2, \ldots, G_{limit}$. BIC [60] is selected since, in the model-based partitioning applications, it has good performance [18, 71]. BIC is estimated based on log likelihood of data as

$$BIC_G = log\ell(\hat{\theta}_G) - (N_{p,G}/2)\log N \tag{4.8}$$

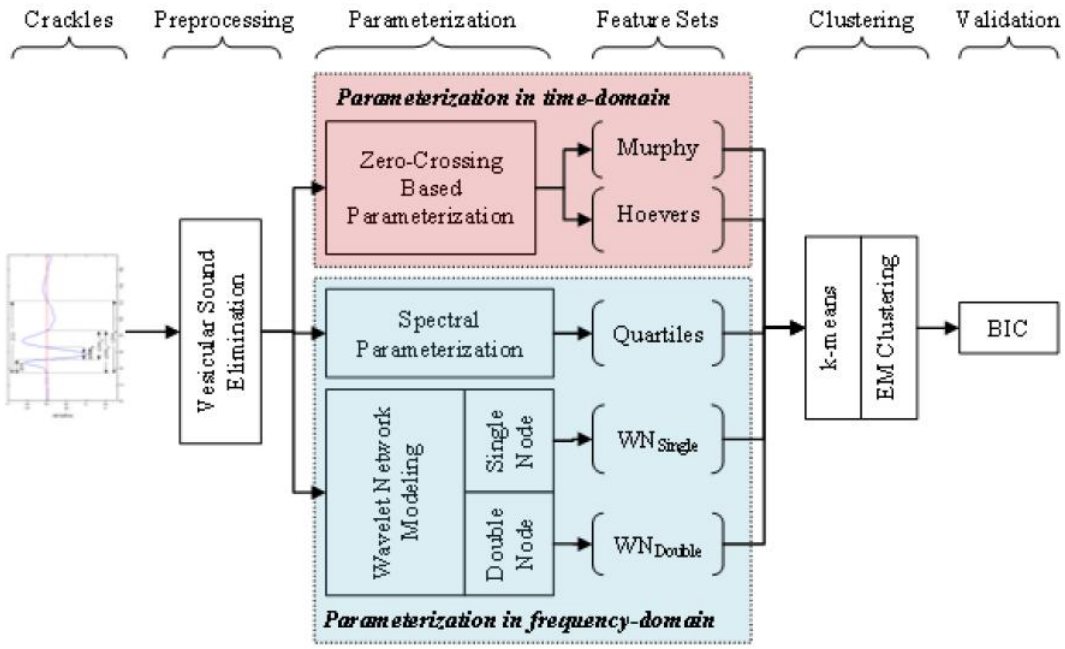

Figure 4.1 Block Diagram of the Clustering Algorithm. Murphy and Hoevers feature sets are in time domain whereas feature sets of quartiles and central frequencies are in frequency domain.

where θ_G represent the estimated cluster parameters, i.e. mean and variance for normal distributions, when the number of clusters is selected as G. $N_{p,G}$ is the total number of estimated independent variables of the parameters corresponding to the summation of Gd and $G(d(d+1)/2)$ variables from the mean vectors and the covariance matrices, respectively [60, 71]. The optimum is the number of clusters at which maximum BIC is reached. The clustering algorithm is summarized in Figure 4.1.

4.2 Results

The parameterization of the crackle waveforms based on zero-crossing, spectral components and WN modeling yields five feature sets. The features belonging to these sets are listed in Table 4.1.

Clustering experiments are performed on all of the feature sets separately and BIC values are compared to determine the optimum number of crackle clusters that convey representative feature values. The cluster likelihood densities and BIC values

Table 4.1
A description of feature sets.

Feature Sets	# Features	Features
Murphy	2	IDW, 2CD
Hoevers	4	LDW_1, LDW_2, LDW_3, LDW_4
Quartiles	2	Q_{Lower}, Q_{Upper}
WN with single node	1	CF
WN with double node	2	CF_1, CF_2

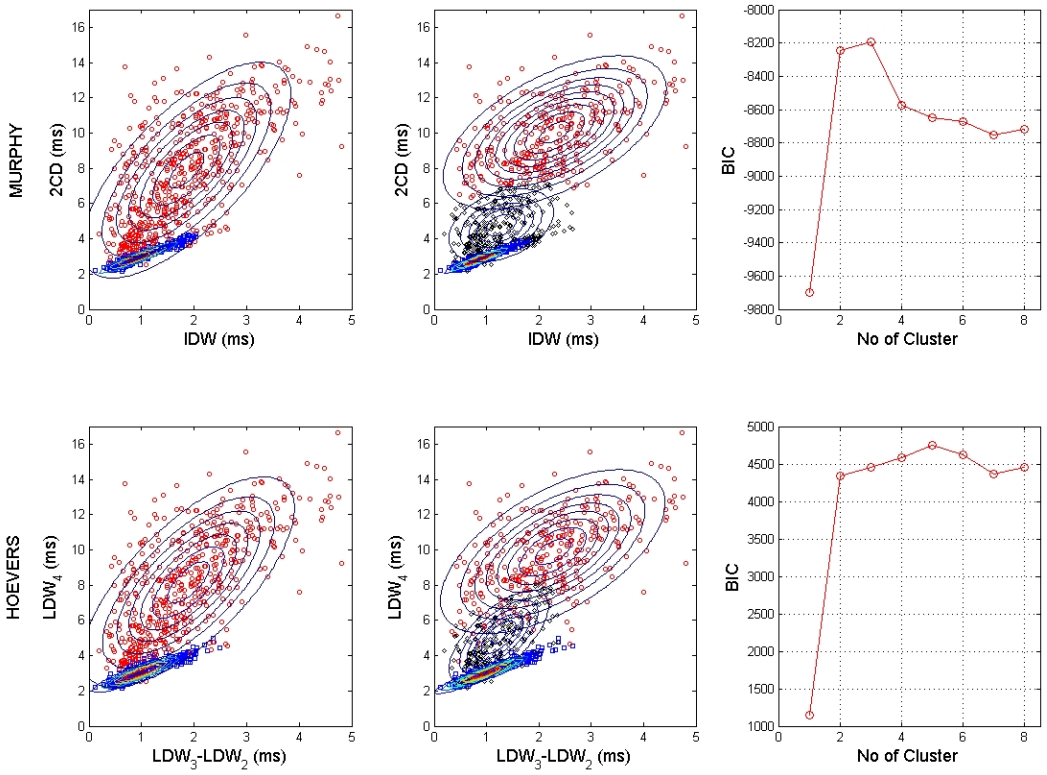

Figure 4.2 The scatter plots of feature samples and isoprobability contours of likelihood densities of clusters estimated using *EM* algorithm according to the feature sets in time domain, i.e. Murphy in the first row and Hoevers in the second row. *BIC* values are depicted in the last column. To comparatively observe the cluster distributions, converted versions of four features of Hoevers corresponding to two features of Murphy are used in the figures whereas the clustering analysis is performed using all the four features. Blue square, red circle, black diamond marks represent the samples labeled as fine, coarse and medium crackles, respectively. (One third of the samples are shown to reduce ink-to-noise ratio.)

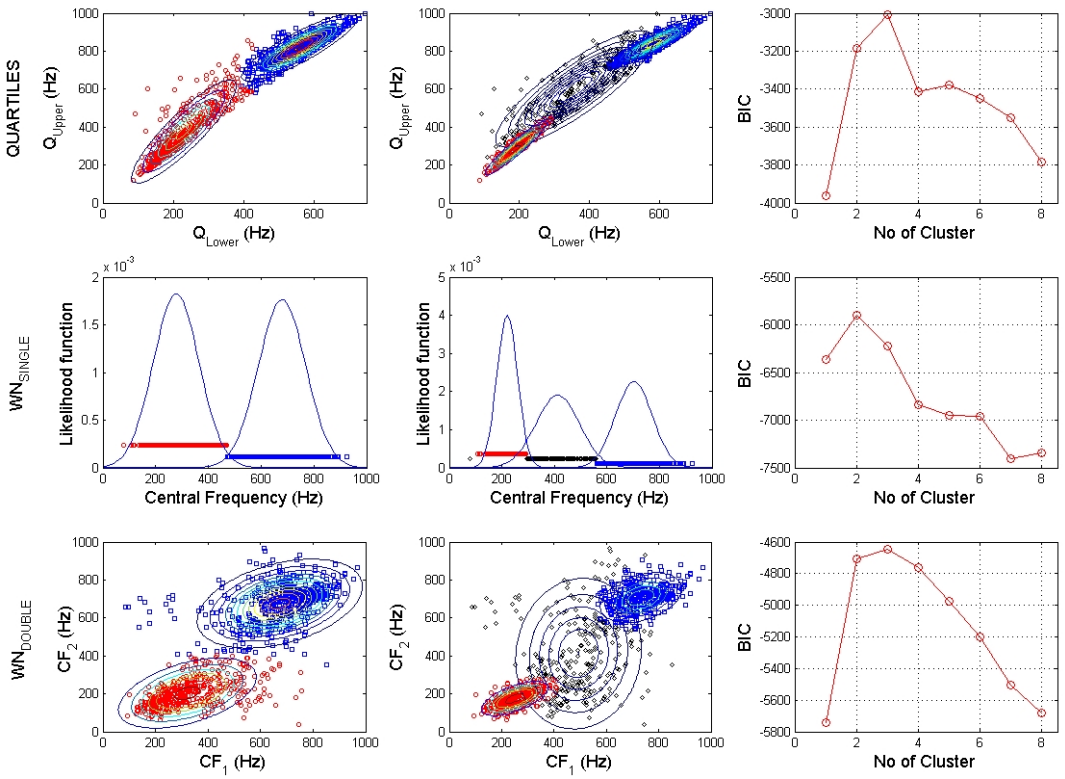

Figure 4.3 Estimated likelihood densities of clusters and *BIC* values according to the feature sets in frequency domain, i.e. quartile frequencies (the first row), central frequencies obtained from modeling using WN with single (the second row) and double (the third node) node.

of clusters are depicted in Figure 4.2 and Figure 4.3. The means of the clusters are the centers of the densities whereas the shape and orientation of isoprobability contours depend on the covariance matrices of clusters. Since unconstrained covariance matrices are employed in the clustering analysis, the shape and orientations of densities can be flexible and diverse for different clusters. For instance, for Murphy feature set in both the two- and three-cluster cases, 'fine' cluster distributes over smaller area with skewed and elongated shape whereas the 'coarse' cluster has wider ellipsoidal distribution. Therefore, the coarse crackles, which distribute over larger areas with lower density than fine crackles, can be labeled more accurately with unconstrained covariance matrices.

BIC values of the clustering analysis using different feature sets imply that there may exist one more cluster in addition to the fine and coarse crackle clusters. *BIC* values of clustering experiments performed on three feature sets, namely Murphy, quartiles and WN double node feature sets, reach the maximum value at the three-

Table 4.2
Mean feature values of the clusters

Sets	Features	Two-Cluster Case		Three-Cluster Case		
		Fine	Coarse	Fine	Medium	Coarse
Murphy	IDW (ms)	0.93±0.41	1.86±1.00	0.87±0.34	1.31±0.56	2.26±1.04
	2CD (ms)	2.93±0.48	7.93±3.0	2.85±0.40	4.78±1.09	10.02±2.09
Hoevers	LDW_1 (ms)	0.70±0.09	1.63±0.65	0.69±0.08	1.03±0.26	1.96±0.57
	LDW_2 (ms)	1.42±0.16	3.83±1.47	1.40±0.14	2.34±0.64	4.64±1.17
	LDW_3 (ms)	2.39±0.51	5.72±2.14	2.37±0.52	3.59±0.94	6.87±1.75
	LDW_4 (ms)	3.02±0.55	8.18±2.97	3.00±0.55	5.08±1.35	9.84±2.32
Quartiles	Q_{Lower} (Hz)	560.2±76.2	229.2±77.7	583.4±61.6	355.7±105.4	187.8±43.6
	Q_{Upper} (Hz)	819.6±84.0	376.6±143.7	841.1±63.2	596.4±143.7	287.2±69.8
WN_{Single}	CF (Hz)	679.3±92.0	277.1±87.7	703.4±71.1	412.6±79.6	218.8±39.2
WN_{Double}	CF_1 (Hz)	673.3±143.6	317.3±125.8	731.7±81.4	484.0±126.8	250.7±64.7
	CF_2 (Hz)	676.1±106.5	202.7±80.5	703.5±68.6	412.6±207.8	174.7±44.5

cluster case, having lower values for the two-cluster case. For the Hoevers set, the BIC values for the two and three-cluster cases are close to each other, being higher for three clusters although the maximum BIC value is reached at five clusters. The maximum BIC value is at the two-cluster case for WN single node feature set. This disparity may be due to loss of information when a crackle, which is composed of progressively widening cycles, is modeled with a single node with larger modeling error compared to that of a double node. To validate the optimum cluster number, AIC which has a tendency to overestimate number of clusters, in contrast to BIC which has a tendency to underestimate, was also calculated and similar results regarding number of clusters were found for each feature set.

The mean values of features that depict the representative crackle of each cluster are listed in Table 4.2, indicating that clusters using different feature sets represent resembling crackle waveforms for each crackle type. As mentioned, Murphy parameters are linearly dependent on Hoevers. For the two-cluster case, corresponding IDW and $2CD$ values of Hoevers features for the fine cluster are 0.97 ms (2.39-1.42) and 3.02 ms, respectively whereas Murphy are 0.93 ms and 2.93 ms. For the coarse clusters, using the same conversion, Hoevers features have the corresponding values of 1.89 ms

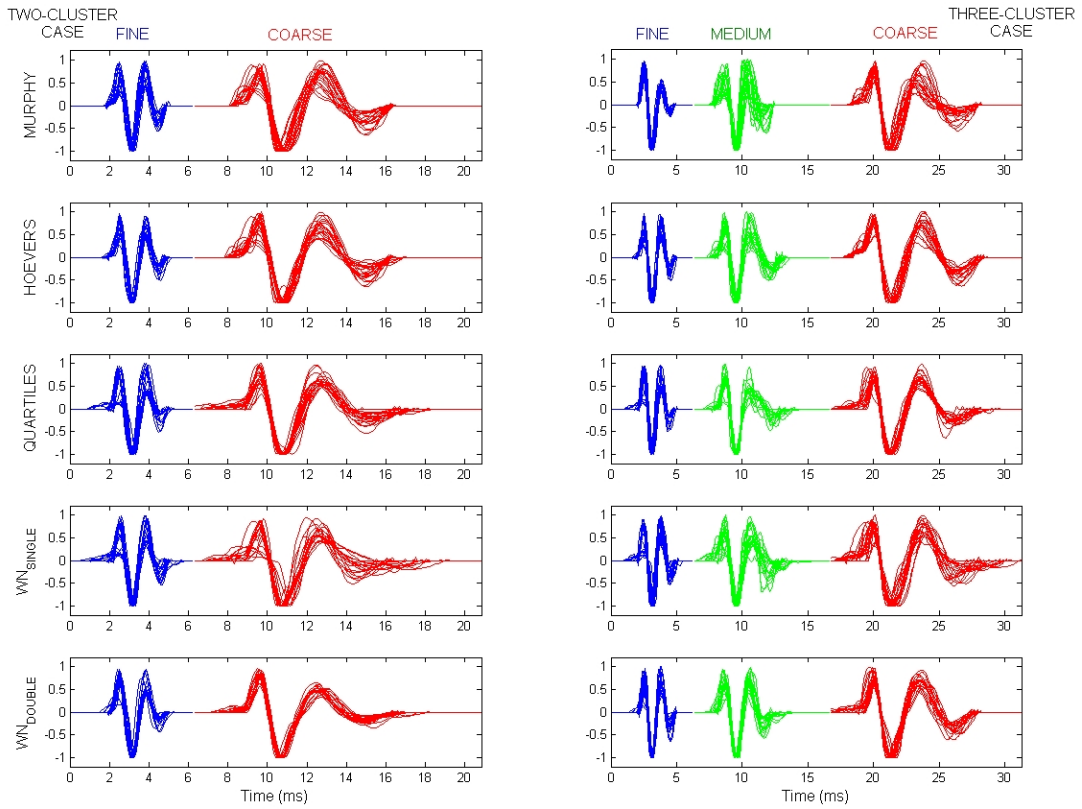

Figure 4.4 Waveforms of the crackles in the 20-nearest neighborhood of the means of the clusters estimated from five feature sets. The typical waveforms of clusters are depicted for two- and three-cluster analysis.

and 8.18 ms whereas, Murphy values are 1.86 ms and 7.93 ms, respectively. For the three-cluster case, fine, medium and coarse clusters have the IDW and $2CD$ values of 0.97 ms and 3.00 ms, 1.25 ms and 5.08 ms, 2.23 ms and 9.84, respectively, according to Hoevers whereas Murphy values are 0.87 and 2.85, 1.31 and 4.78, 2.26 and 10.02, respectively.

Moreover, the CFs can be approximately estimated using $2CD$ values by the relation of $CF \leftarrow 1/2CD$. The estimated CFs using Murphy mean values of clusters are 683 Hz and 252 Hz for the two clusters whereas they are 701.8Hz, 418.4Hz and 199.6Hz for the fine, medium and coarse clusters. A similar comparison between the mean of the lower and upper quartile frequencies and CFs can be made where they are 689.9 Hz and 302.9 for the two-cluster case and 712.3 Hz, 476.1 Hz and 237.5 Hz for the three-cluster case. As these figures demonstrate, clusters have comparable crackle parameter values regardless of the feature set. To better visualize the typical crackle waveforms corresponding to each cluster, 20 nearest crackles to the mean of

Table 4.3
Confusion matrices for (a) two- and (b) three-cluster analyses. The confusion matrices on the diagonal of the table shows the numbers of samples labeled as fine, medium and coarse crackles. The off-diagonal confusion matrices show the true and false matching of labeling according to different feature sets. (F: Fine, M: Medium and C: Coarse)

(a)		Murphy		Hoevers		Quartiles		WN_{Single}		WN_{Double}	
		F	C	F	C	F	C	F	C	F	C
Murphy	F	997	0	978	19	987	10	992	5	996	1
	C	0	1714	118	1596	315	1399	448	1266	324	1390
Hoevers	F	978	118	1096	0	1088	8	1095	1	1096	0
	C	19	1596	0	1615	214	1401	345	1270	224	1391
Quartiles	F	987	315	1088	214	1302	0	1301	1	1253	49
	C	10	1399	8	1401	0	1409	139	1270	67	1342
WN_{Single}	F	992	448	1095	345	1301	139	1440	0	1289	151
	C	5	1266	1	1270	1	1270	0	1271	31	1240
WN_{Double}	F	996	324	1096	224	1253	67	1289	31	1320	0
	C	1	1390	0	1391	49	1342	151	1240	0	1391

(b)		Murphy			Hoevers			Quartiles			WN_{Single}			WN_{Double}		
		F	M	C	F	M	C	F	M	C	F	M	C	F	M	C
Mur	F	902	0	0	871	31	0	841	61	0	889	13	0	828	74	0
	M	0	797	0	154	560	83	196	537	64	363	407	27	149	577	71
	C	0	0	1012	0	68	944	0	194	818	4	243	765	0	123	889
Hov	F	871	154	0	1025	0	0	928	97	0	1012	13	0	888	137	0
	M	31	560	68	0	659	0	105	454	100	221	417	21	87	465	107
	C	0	83	944	0	0	1027	4	241	782	23	233	771	2	172	853
Qua	F	841	196	0	928	105	4	1037	0	0	1037	0	0	911	126	0
	M	61	537	194	97	454	241	0	792	0	219	500	73	66	606	120
	C	0	64	818	0	100	782	0	0	882	0	163	719	0	42	840
WN_S	F	889	363	4	1012	221	23	1037	219	0	1256	0	0	977	279	0
	M	13	407	243	13	417	233	0	500	163	0	663	0	0	453	210
	C	0	27	765	0	21	771	0	73	719	0	0	792	0	42	750
WN_D	F	828	149	0	888	87	2	911	66	0	977	0	0	977	0	0
	M	74	577	123	137	465	172	126	606	42	279	453	42	0	774	0
	C	0	71	889	0	107	853	0	120	840	0	210	750	0	0	960

each cluster are plotted in Figure 4.4. These plots, representative waveforms for each type of crackle, i.e. fine, medium and coarse, likewise, display similar characteristics irrespective of which feature set is used.

The confusion matrices that indicate the matching of labeling results of clustering experiments using different feature sets are shown in Table 4.3. In confusion matrices, each comparison between two feature sets is interpreted as 2-to-2 and 3-to-3 matrices for two- and three-cluster cases, respectively. Each table consists of 5-to-5 matrices of these confusion matrices. The confusion matrices on the diagonals of tables show the number of cluster members labeled using the corresponding feature sets.

Table 4.4
Accuracies of clustering results that are the ratios between the numbers of true-matched samples to the total number of samples.

	Two-Cluster Case					Three-Cluster Case				
	Murphy	**Hoevers**	**Quartiles**	**WN_{Single}**	**WN_{Double}**	**Murphy**	**Hoevers**	**Quartiles**	**WN_{Single}**	**WN_{Double}**
Murphy	100.0%	95.0%	88.0%	83.3%	88.0%	100.0%	87.6%	81.0%	76.0%	84.6%
Hoevers	95.0%	100.0%	91.8%	87.2%	91.7%	87.6%	100.0%	79.8%	81.2%	81.4%
Quartiles	88.0%	91.8%	100.0%	94.8%	95.7%	81.0%	79.8%	100.0%	83.2%	86.9%
WN_{Single}	83.3%	87.2%	94.8%	100.0%	93.3%	76.0%	81.2%	83.2%	100.0%	80.4%
WN_{Double}	88.0%	91.7%	95.7%	93.3%	100.0%	84.6%	81.4%	86.9%	80.4%	100.0%

There are, for instance, 1025 fine, 659 medium, and 1027 coarse crackles in the dataset resulting from clustering experiments using Hoevers feature set. The off-diagonal confusion matrices of tables indicate the matching between clustering using two different feature sets. The values on the diagonal of a confusion matrix show the number of true matched crackles whereas the off-diagonal values indicate false matching. For example, 560 of 659 medium labeled crackles of Hoevers are true-matched whereas 31 and 68 of 659 medium crackles are labeled as fine and coarse, respectively, using Murphy set.

The accuracies in Table 4.4 indicate the true-matching ratios between feature sets. The accuracies are defined as the ratio of the sum of the quantities on the diagonal of a confusion matrix to the total number of crackles, namely 2711. For two-cluster case, true matching between clustering experiments on four feature sets is achieved for more than 88% of crackles reaching maximum value 95.7%. For the fourth feature set, namely single node wavelet model, lower figures such as 83.3% are realized, owing to the relatively higher modeling error. For the three-cluster case, true matching rate is also high ranging between 79.8% and 87.6%, except for the single node wavelet model whose rate is between 76.0% and 83.2%.

5. CONCLUSIONS

A new automatic method has been proposed in Chapter 2 for the elimination of background VSs from crackle signal with minimum distortion of crackle parameters which are important in the diagnosis of respiratory disorders. A region of interest is designated and a distortion metric based on the correlation between raw and filtered waveforms in that region is defined. Cut-off frequency is estimated based on the DT metric. Furthermore, to reduce computational cost, a regression analysis is realized which predicts a new cut-off frequency, fitted cut-off frequency, from estimated cut-off frequency based on percentiles of cPS of the crackle signal. As a comparison basis, wavelet filtering is also applied on the same data.

The algorithm is validated on simulated crackles with known parameters which are superimposed on recorded VSs from healthy subjects and have, therefore, deformed parameters. A very low error rate is achieved in filtered crackles with estimated cut-off frequency for both FCs and CCs. The error rate results of filtering with fitted cut-off frequency were slightly higher with almost ten times faster computational time, a result which justifies slightly higher error rate for a much smaller computational cost. Both filters perform at least twice better than wavelet filters.

The application of the algorithm on real crackles from subjects with various respiratory disorders also showed how transformed the crackle parameters were after the method was applied thus emphasized the significance of the shape of the waveform in crackle studies. The algorithm is promising since it renders itself to computerized analysis of pulmonary sounds with the final aim of building a diagnosis system. A sensitivity analysis made on the crackle parameters indicates the significance of proper filtering in view of parameter values which are essential in such a diagnosis system.

In Chapter 3, crackles are modeled in time-frequency domain using the WNs. Wavelets not only have the oscillating waveform like sinusoid signals with variable

frequency but also have finite energy that is concentrated in a time interval. Wavelets, therefore, have the ability of representing a transient signal with lower number of components. In our application, WN-based parameterization offers the advantage of coding crackles with a relatively small number of parameters that can be used to faithfully regenerate them without the loss of waveform morphology. In other words, crackles can be interpreted in time and frequency domains using WN modeling by representing the signal with WN parameters whose number equals to five times the number of WN nodes. In our study, minimal error rates have been obtained for a wide range of crackle types with two node WNs. Moreover the extracted features from WN model parameters have been shown to be consistent with the more conventionally used parameters based on zero-crossings in two-class clustering experiments.

In the future, as an extension of the study in Chapter 3, some specific base wavelets (atoms) may be defined based on the characteristics of crackle types and may be employed in the detection of the crackles in the pulmonary sound signals using the matching pursuit method [39]. The fine tuning of the parameters can be performed using WN after the detection. Therefore, the computerized crackle-based analysis of pulmonary disorders can be achieved with the information of localization and classification of the crackle.

In Chapter 4, a set of clustering experiments have been carried out on a database of pulmonary crackles with an aim to probe the existence of a third crackle type, medium, besides the traditionally accepted types, namely, fine and coarse crackles. Moreover, the representative parameter values for each crackle type have been explored. A model based clustering algorithm, the EM algorithm, is used and the resulting cluster numbers are validated with BIC. Five different feature sets are extracted from the preprocessed crackle samples, two of which are conventional parameters that have been suggested by Murphy et al. and Hoevers et al. and that are derived from the zero-crossings of crackle waveforms. The third feature set corresponds to the spectral components of the crackles whereas the remaining two sets are derived from a single- and double-node WN modeling.

The results of the clustering experiments demonstrate strong evidence for the existence of a third crackle type. Moreover, the labels yielded by clustering experiments using different feature sets match for roughly 80% or more of the crackle samples, resulting in similar representative crackle parameter values for all feature sets. For the time-domain parameters, namely IDW and $2CD$, approximate values are 2.2 ms and 10.0 ms for coarse crackles, 1.3 ms and 5.0 ms for medium crackles and finally, 0.9 ms and 3.0 ms for fine crackles. These results correlate closely with ATS definitions which classify crackles with $2CD$ value of approximately 10 ms as coarse and crackles with $2CD$ of less than 5 ms as fine. This study clusters the undefined zone in ATS standards as medium. For the frequency domain parameters, approximate values for the central frequencies are 200 Hz, 400 Hz and 700 Hz for coarse, medium and fine crackles, respectively. Since the crackle classification algorithm employed in this study is unsupervised, this method makes the evaluation of crackles more objective, rendering this approach to be used in computerized analysis of pulmonary sounds. In future studies, various pulmonary pathologies may be correlated with the three different crackle types and the findings may be utilized in constructing databases with the final aim of building a computerized diagnosis system.

APPENDIX A. THE RESPIRATORY SYSTEM AND THE LUNGS

A.1 The Respiratory System

Most of the body cells consume oxygen and generate carbon dioxide in energy production. The function of the respiratory system is to supply oxygen from external environment and remove carbon dioxide from body. The oxygen - carbon dioxide exchange (respiration) is accomplished by following complementary processes: (1) the expiration of the air with high carbon dioxide concentration and inspiration of the air with high oxygen concentration from environment, (2) the gas exchange between pulmonary capillaries and alveoli, named external respiration, (3) the oxygen-carbon dioxide transport in blood, and (4) the gas exchange between the tissue cells and blood, named internal respiration [38, 61]. The first two processes are carried out by conductive airways and the lungs. The journey of inspired air starts from nasal or oral cavity and continue through the pharynx, the larynx, the trachea, the bronchi, and the lungs as shown in Figure A.1.

A.2 The Lungs

The lungs are cone-shaped organs located in the thoracic cavity. They extend from the diaphragm to a point about 2.5 cm above of the clavicle. They are enclosed by double-layer pleural membrane whose outer layer is attached to the wall of thoracic cavity and inner layer is attached to the lungs. The lungs are divided into lobes by deep, oblique fissures. There are three lobes, i.e. superior, middle and inferior, in the right lung whereas two lobes, i.e. superior and inferior, in the left lung. Each lobe is divided into lobules that are ten in the right lung and nine in the left lung.

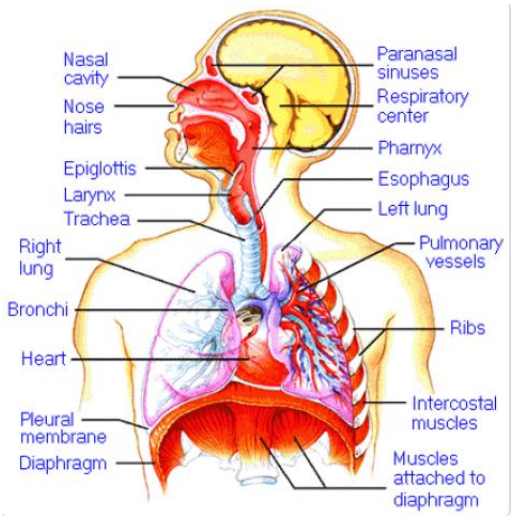

Figure A.1 The respiratory system (http://www.medem.com)

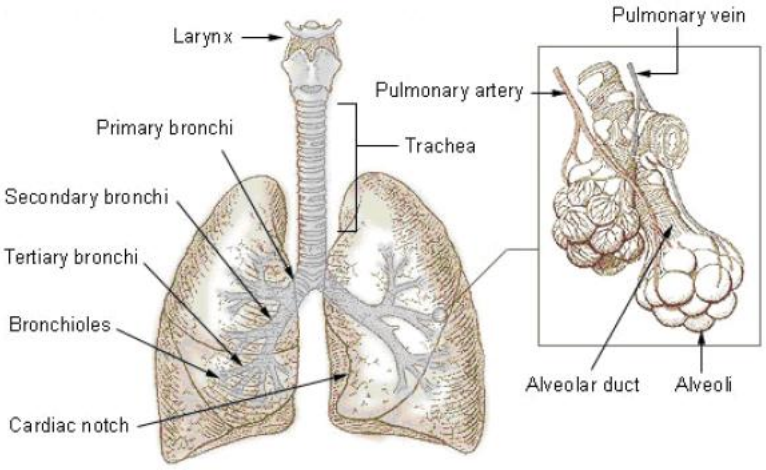

Figure A.2 The lungs and tracheobronchial tree

A.3 Bronchial Tree

The trachea is divided into right and left primary bronchi that contain C-shaped cartilage like the trachea. Each bronchus gives rise to secondary bronchus for each lobe and each secondary bronchus subdivided into tertiary bronchus for each lobule. Tertiary bronchi continue to subdivide into bronchioles, terminal bronchioles and respiratory bronchioles, gradually. Respiratory bronchiole gives rise to alveolar ducts that are surrounded by many alveoli and alveolar sacs. The structure depicted in Figure A.2 acquired from *http* : *//training.seer.cancer.gov*. The branching structure from the trachea up to terminal bronchioles is named the bronchial tree. Oxygen - carbon dioxide exchange between pulmonary capillaries and air does not occur in the bronchial tree. The main location of the gas exchange is in the alveoli although some occurs in the alveolar ducts and respiratory bronchioles [61, 67].

The structure of the upside-down tree changes as the branching becomes more extensive. The cartilage layers in trachea replace incomplete cartilage rings in primary bronchi and disappear gradually in subdivided airways. There is no cartilage in smallest bronchioles. As the amount of cartilage decreases, the amount of smooth muscle increases.

APPENDIX B. THE PULMONARY DISEASES WITH AUSCULTATION FINDINGS

There are many types of pulmonary diseases. In this section, some diseases that can be diagnosed via auscultation are briefly described. Some of these diseases, i.e. interstitial pulmonary fibrosis and sarcoidosis, cause a reduction the expansion ability of the lungs and a decrease in the total amount of air that the lungs can hold. A disease in this class is named restrictive diseases. Some diseases, i.e. asthma, chronic bronchitis, emphysema, COPD, and bronchiectasis, give rise to a reduction in the amount and the rate of the air that can be expired. A disease in this class is named obstructive diseases.

B.1 Asthma

Asthma is an inflammatory disease that affects the airways. Inflammation makes inside walls of airways sensitive, thus they respond strongly to allergenic and irritating effects. When asthma attack occurs, the bronchioles are constricted due to the contraction of bronchial smooth muscles and tenacious mucus is produced [9]. The phenomena cause the reduction of airflow. The characteristics of asthma are wheezing, cough, shortness of breath and chest tightness.

B.2 Emphysema

Emphysema has two types, i.e. panlobular and centrilobular. Panlobular emphysema is a condition characterized by the destruction of the wall between alveoli or air ducts which gives rise to permanent abnormal enlarged air spaces. This reduces the interaction surface between blood and air. The elasticity of lung tissues is reduced and the ability of stretch and recoil of the lungs is impaired. Panlobular emphysema

is characterized by a hyper inflated chest. In centrilobular emphysema, the respiratory bronchioles are destroyed [31]. The air is trapped within the alveoli due to the bronchial collapse during expiration and the gas exchange cannot be accomplished. The symptoms of emphysema are shortness of breath and cough.

B.3 Chronic Bronchitis

Chronic bronchitis is a condition where the inflammation in the lining of bronchi occurs, reducing airflows and secreting tenacious mucus. The disease is defined by the prolonged mucus-producing cough. The inflammation gives rise to scarring of the line of bronchi. There is a gradual process that starts with prolonged irritation of the bronchial tubes and accompanied by excessive mucus secretion, then continues with thickening of walls of bronchi and increasing of cough, and concludes with the structural changes and the scarring in the bronchi.

B.4 Chronic Obstructive Pulmonary Diseases (COPD)

COPD is referred to an airway obstruction that is a various combination of chronic bronchitis, emphysema and asthma. These diseases concur frequently and it is difficult to decide on which disease leads the obstruction. The interrelationship between these three diseases is depicted in Figure B.1 acquired from [9].

B.5 Bronchiectasis

The characteristics of bronchiectasis are the destruction and inflammation of bronchial wall, damage of ciliated cells and increase of mucus secretion that is shown in Figure B.2 acquired from $http://www.merck.com$. The elasticity of bronchial wall reduces and bronchi become wider. The destructed walls promote mucus production

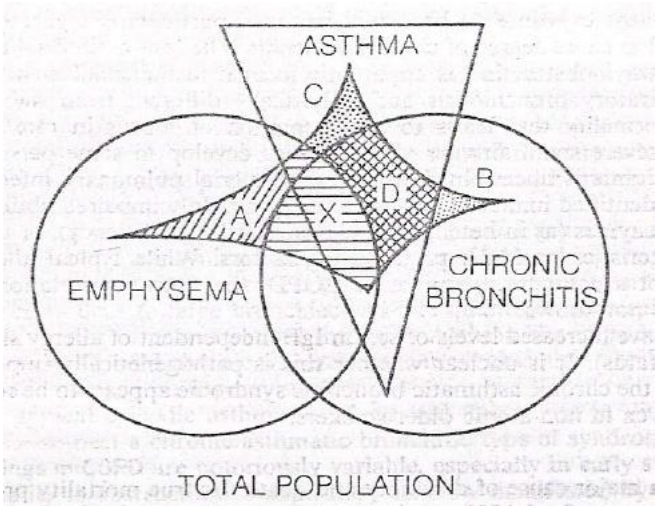

Figure B.1 the Interrelationship between asthma, chronic bronchitis, emphysema and COPD. Shaded area represents subjects with COPD.

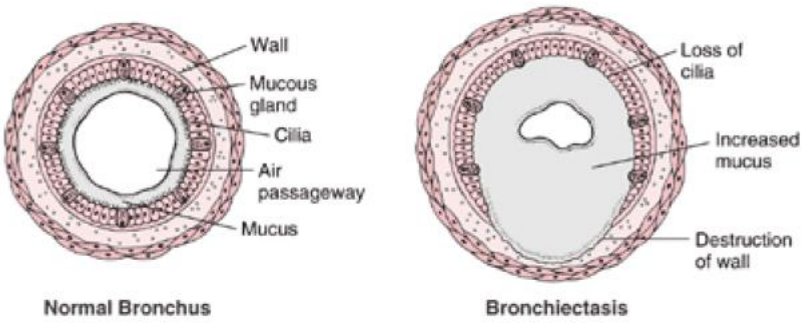

Figure B.2 The effects of bronchiectasis on airways and bronchial walls

that obstructs airways and accumulates bacteria. The infection in the upper airways can extend to the lower airways and alveoli, leading to pneumonia and scarring. There are three types of bronchiectasis, i.e. cylindrical, varicose and cystic. The cylindrical is most common and reversible. The airways dilate slightly. In the varicose, some parts of bronchial walls extend and are destructed. The cystic is most severe and produces ballooning in the bronchi. The symptoms of bronchiectasis are coughing, shortness of breath, weakness and abnormal chest sounds.

B.6 Interstitial Pulmonary Fibrosis

The terms interstitial pulmonary fibrosis, interstitial lung diseases and pulmonary fibrosis are generally used to describe the same condition. The term "interstitial" comes from the interstitium that is the name of the tissue between alveoli. "Fibrosis" means scarring. There are probably 130 - 200 related diseases that are called pulmonary fibrosis and show similar characteristics. They all begin with inflammation and lead to scarring (fibrosis). The inflammation influence various parts of the lungs, i.e. the walls of bronchioles (bronchiolitis), the walls of alveoli (named alveolitis), and pulmonary capillaries (named vasculitis). The symptoms are breathlessness during exercise and a dry cough.

B.7 Sarcoidosis

Sarcoidosis is characterized by inflammation and the presence of granulomas, small areas of inflamed cells. Granulomas may appear on walls of alveoli, bronchial wall and lymph node in the chest. Sarcoidosis reduces lung volume and elasticity of lung tissues. Its symptoms are a dry cough, shortness of breath and wild thoracic pain.

B.8 Pneumonia

Pneumonia is infection or inflammation of the lungs caused by a bacterium, a virus or a fungus. Pneumonia is classified as two types according to the location of appearance in the lungs. Lobar pneumonia appears on a lobe of the lungs whereas bronchial pneumonia affects both lungs. The symptoms are shortness of breath, cough, fever, chill and increase in mucus production.

APPENDIX C. AUSCULTATION AND ADVENTITIOUS SOUNDS

Respiratory sounds consist of all sounds related to respiration, e.g. breath sounds, adventitious sounds, cough sounds, snoring sounds, and sounds which stem from the respiratory muscles. Voiced sounds during breathing are not included in respiratory sounds [64]. Respiratory sounds can distinctively indicate the healthy and pathological conditions and they have been used for diagnosis since ancient times. Especially after the invention of the stethoscope by Laennec, the importance of auscultation in diagnosis has increased. He describes the breath sounds heard over the chest as "a distinct murmur corresponding to the flow of air into and out of air cells" [36]. However, the origin of the sounds is not completely certain and, probably, multiple mechanisms are involved. The lung sounds cannot be generated by lung itself if there is no airflow. The turbulence of the air at the level of bronchi probably induces them. Because the gas velocity decreases and is at less than critical level to induce turbulence, the airflow is silent in smaller bronchi [65]. Pasterkamp et al. [51] reported the major types and characteristics of respiratory sounds as in Table C.1.

C.1 Normal Lung Sounds

The respiratory sounds of healthy subject heard over the chest are named "normal lung sounds". The peak frequency of normal lung sounds is usually below 100 Hz and it is very difficult to distinguish them from muscular and cardiovascular sounds. The energy of normal lung sounds decrease sharply between 100 and 200 Hz; however, they can still be detected at about 1000 Hz using sensitive microphones [51].

Table C.1
Major categories of pulmonary sounds [2].

Respiratory Sound		Mechanisms	Origin	Acoustics	Relevance
Basic sounds	Normal lung sound	Turbulent flow vortices, unknown mechanisms	Central airways (expiration), lobar to segmental airway (inspiration)	Low-pass filtered noise (range <100 to >1,000 Hz)	Regional ventilation, airway caliber
	Normal tracheal sound	Turbulent flow, flow impinging on airway walls	Pharynx, larynx, trachea, large airways	Noise with resonances (range <100 to > 3,000 Hz)	Upper airway configuration
Adventitious sounds	Wheeze	Airway wall flutter, vortex shedding	Central and lower airways	Sinusoid (range ~100 to >1,000 Hz; duration, typically>80 ms)	Airway obstruction, flow limitation
	Rhonchus	Rupture of fluid films, airway wall vibrations	Larger airways	Series of rapidly dampened sinusoids (typically<300 Hz and duration>100 ms)	Secretions, abnormal airway collapsibility
	Crackle	Airway wall stress-relaxation	Central and lower airways	Rapidly dampened wave deflection (duration typically < 20 ms)	Airway closure, secretions

C.2 Adventitious Sounds

In pathological conditions, additional respiratory sounds (called adventitious sounds) are superimposed over the normal lung sounds. They are divided into two main groups, namely transient and continuous adventitious sounds. The transient sounds, crackles, are explosive sounds heard mostly during inspiration rather than during expiration. The continuous adventitious sounds, namely wheeze and rhonchus, are musical and sinusoidal sounds.

C.2.1 Crackles

Crackles are discontinuous type of adventitious sounds that occur in pathological conditions and are superimposed on normal breath sounds. Crackles are explosive and transient in character, and occur frequently in cardio-respiratory diseases [54]. They generally start with a sharp deflection and continue with a damped and progressively

wider sinusoidal wave [46]. Their duration is less than 20ms and their frequency range is from 100 to 2000 Hz or even higher [20, 48]. They are distinguished into two types, i.e. fine and coarse. The former are related with interstitial lung diseases, whereas the latter are generally associated with obstructive diseases. The generating mechanism of crackles is not known with certainty. There are two assumptions for the source of energy to generate crackles: (1) pressure equalization [17] and (2) change in elastic stress ([19] after explosive opening of small airways that are abnormally closed by surface forces because of pathological dysfunction.

C.2.2 Wheezes

Wheezes are continuous type of adventitious sounds. Since their waveforms are sinusoidal, they also called musical. According to guidelines of a project of European Union, the dominant frequency components of wheezes are generally higher than 100 Hz whereas their durations are higher than 100 ms [64]. Wheezes can show monophonic and polyphonic frequency characteristics.

American Thoracic Society (ATS) nomenclature [5] divides continuous adventitious sounds into two categories, i.e. wheeze and rhonchus. Wheezes are higher-pitch and their dominant frequencies are defined as higher than 400 Hz whereas dominant frequency components of rhonchi are defined as lower than 200 Hz. The source of wheezing sound is assumed to be oscillating airway walls. Grotberg and Davis [22] modeled the generating mechanism and concluded that wheeze generation is correlated with airflow threshold. Although airflow should reach a critical value for generating wheeze, the reaching critical value does not always generate a wheeze.

Since lung tissue behaves like low-pass filter in lung sound transmission [70], wheezes with high frequency components can be auscultated better over the trachea than at the chest wall. As reported by Sovijarvi et al. [65], in the studies performed by Baughman and Loudon [7, 6], the dominant highest frequency of wheezes auscultated from the chest wall is 710 Hz. Furthermore, Fenton et al. [16] state that the

wheezes with the peak frequency at 870 and 940 Hz can be auscultated over the trachea, although they are not audible at the chest wall. Fenton at al. use lung sounds simultaneously acquired from the trachea and the chest wall in their study.

APPENDIX D. THE LOCATIONS OF THE MICROPHONES ON THE POSTERIOR CHEST WALL

Pulmonary sound signals are recorded using 14 air-coupled electret microphones. They are embedded in capsules that supply air cavity between skin and microphones. The air cavity is designed to be sensitive to the spectral components of pulmonary sounds [35]. The locations of microphones at the chest are determined according to the advices given by clinicians. The microphones are located according to the locations used in clinical auscultation from the posterior chest wall. Seven microphones are located at each left and right side of the chest wall symmetrically around the spine that is depicted in Figure D.1. The figure is acquired from Sen's MS Thesis [62].

The first two microphones at the top are located at the level of the clavicles. The other microphones are located according to the first two microphones. The distance between the first two microphones is 6 cm. The distances between microphones in the nearby spine are enlarged gradually and, in base, the distance reaches 12 cm. The distance between two adjacent microphones at the same level is adjusted as 6 cm whereas the distance between microphone levels is 7 cm. The details of DAQ system are described in [62].

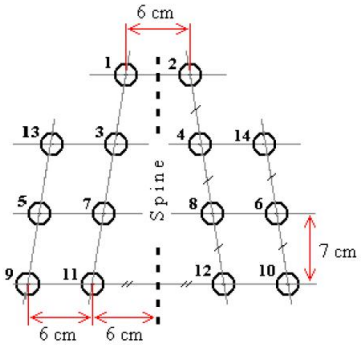

Figure D.1 The microphone locations on the posterior chest wall

REFERENCES

1. E. Ademovic, J. C. Pesquet, and G. Charbonneau. Time-scale segmentation of respiratory sounds. *Technol Health Care*, 6(1):53–63, Jun 1998.

2. M. Akay. *Time Frequency and Wavelets in Biomedical Signal Processing.* IEEE Press, 1998.

3. N. al Jarad, S. W. Davies, R. Logan-Sinclair, and R. M. Rudd. Lung crackle characteristics in patients with asbestosis, asbestos-related pleural disease and left ventricular failure using a time-expanded waveform analysis–a comparative study. *Respir Med*, 88(1):37–46, Jan 1994.

4. E. Alpaydin. *Introduction to Machine Learning.* MIT Press, 2004.

5. ATS. Updated nomenclature for membership reaction. reports of the ats-accp ad hoc committee. *Am Thorac Soc News*, 3:5–6, 1977.

6. R. P. Baughman and R. G. Loudon. Quantitation of wheezing in acute asthma. *Chest*, 86(5):718–722, Nov 1984.

7. R. P. Baughman and R. G. Loudon. Lung sound analysis for continuous evaluation of airflow obstruction in asthma. *Chest*, 88(3):364–368, Sep 1985.

8. R. P. Baughman, R. T. Shipley, R. G. Loudon, and E. E. Lower. Crackles in interstitial lung disease. comparison of sarcoidosis and fibrosing alveolitis. *Chest*, 100(1):96–101, Jul 1991.

9. R. Berkow and A. Fletcher, editors. *the Merck Manual of Diagnosis and Therapy.* Merck & Co.: Rahway, N.J., 1987.

10. C. Burrus, R. Gopinath, and H. Guo. *Introduction to Wavelets and Wavelet Transforms: A Primer.* Prentice Hall, 1997.

11. G. Celeux and G. Govaert. A classification em algorithm for clustering and two stochastic versions. *Comput Statist Data Anal*, 14:315–332, 1992.

12. J. P. Couderc, P. Chevalier, J. Fayn, P. Rubel, and P. Touboul. Identification of post-myocardial infarction patients prone to ventricular tachycardia using time-frequency analysis of qrs and st segments. *Europace*, 2(2):141–153, Apr 2000.

13. A. Dempster, N. Laird, and D. Rubin. Maximum likelihood from incomplete data via the em algorithm. *Journal of the Royal Statistical Society, B*, 39:1–38, 1977.

14. H. Dickhaus and H. Heinrich. Ep parametrization and classification using wavelet networks–theoretical concept and medical application. *Stud Health Technol Inform*, 43 Pt B:541–545, 1997.

15. H. Fastl and E. Zwicker. *Psychoacoustics: Facts and Models.* Springer, 3 edition, 2006.

16. T. R. Fenton, H. Pasterkamp, A. Tal, and V. Chernick. Automated spectral characterization of wheezing in asthmatic children. *IEEE Trans Biomed Eng*, 32(1):50–55, Jan 1985.

17. P. Forgacs. Crackles and wheezes. *Lancet*, 2(7508):203–205, Jul 1967.

18. C. Fraley and E. Raftery. Model-based clustering, discriminant analysis, and density estimation. *J Am Stat Assoc*, 97:611–631, 2002.

19. J. J. Fredberg and S. K. Holford. Discrete lung sounds: crackles (rales) as stress-relaxation quadrupoles. *J Acoust Soc Am*, 73(3):1036–1046, Mar 1983.

20. N. Gavriely and D. Cugell. *Breath Sounds Methodology*. CRC Press, 1995.

21. N. Gavriely, M. Nissan, A. H. Rubin, and D. W. Cugell. Spectral characteristics of chest wall breath sounds in normal subjects. *Thorax*, 50(12):1292–1300, Dec 1995.

22. J. B. Grotberg and S. H. Davis. Fluid-dynamic flapping of a collapsible channel: sound generation and flow limitation. *J Biomech*, 13(3):219–230, 1980.

23. L. J. Hadjileontiadis and S. M. Panas. Separation of discontinuous adventitious sounds from vesicular sounds using a wavelet-based filter. *IEEE Trans Biomed Eng*, 44(12):1269–1281, Dec 1997.

24. H. Heinrich, H. Dickhaus, A. Rothenberger, V. Heinrich, and G. H. Moll. Single-sweep analysis of event-related potentials by wavelet networks–methodological basis and clinical application. *IEEE Trans Biomed Eng*, 46(7):867–879, Jul 1999.

25. H. Heinrich, G. H. Moll, H. Dickhaus, V. Kolev, J. Yordanova, and A. Rothenberger. Time-on-task analysis using wavelet networks in an event-related potential study on attention-deficit hyperactivity disorder. *Clin Neurophysiol*, 112(7):1280–1287, Jul 2001.

26. J. Hoevers and R. G. Loudon. Measuring crackles. *Chest*, 98(5):1240–1243, Nov 1990.

27. L. D. Hudson, R. D. Conn, R. Matsubara, and A. Pribble. Rales-diagnostic uselessness of qualitative adjectives. *Am Rev Respir Dis*, 3113(1):187, Jan 1976.

28. L. Jiao, J. Pan, and Y. Fang. Multiwavelet neural network and its approximation properties. *IEEE Trans Neural Netw*, 12(5):1060–1066, 2001.

29. Y. P. Kahya, M. Yeginer, and B. Bilgic. Classifying respiratory sounds with different feature sets. *Conf Proc IEEE Eng Med Biol Soc*, 1:2856–2859, 2006.

30. A. Kandaswamy, C. S. C. S. Kumar, R. P. Ramanathan, S. Jayaraman, and N. Malmurugan. Neural classification of lung sounds using wavelet coefficients. *Comput Biol Med*, 34(6):523–537, Sep 2004.

31. B. Karnath and M. Boyars. Pulmonary auscultation. *Hospital Physician*, 38:22–26, 2002.

32. T. Katila, P. Piirilä, K. Kallio, E. Paajanen, T. Rosqvist, and A. R. Sovijärvi. Original waveform of lung sound crackles: a case study of the effect of high-pass filtration. *J Appl Physiol*, 71(6):2173–2177, Dec 1991.

33. T. Kawamura, T. Matsumoto, N. Tanaka, S. Kido, Z. Jiang, and N. Matsunaga. Crackle analysis for chest auscultation and comparison with high-resolution ct findings. *Radiat Med*, 21(6):258–266, 2003.

34. H. Kiyokawa, M. Greenberg, K. Shirota, and H. Pasterkamp. Auditory detection of simulated crackles in breath sounds. *Chest*, 119(6):1886–1892, Jun 2001.

35. S. S. Kraman, G. R. Wodicka, Y. Oh, and H. Pasterkamp. Measurement of respiratory acoustic signals. effect of microphone air cavity width, shape, and venting. *Chest*, 108(4):1004–1008, Oct 1995.

36. R. Laënnec. *A treatise on the disease of the chest.* Number 281–384. Hafner Publishing Co., 1962.

37. S. Lehrer. *Understanding Lung Sounds (3rd ed.).* W.B. Saunders, 2002.

38. M. Levitzky. *Pulmonary Physiology.* McGraw-Hill, 6 edition, 2003.

39. S. Mallat and Z. Zhang. Matching pursuits with time-frequency dictionaries. *IEEE Trans Signal Process*, 41(12):3397–3415, Dec. 1993.

40. L. P. Malmberg, A. R. Sovijärvi, E. Paajanen, P. Piirilä, T. Haahtela, and T. Katila. Changes in frequency spectra of breath sounds during histamine challenge test in adult asthmatics and healthy control subjects. *Chest*, 105(1):122–131, Jan 1994.

41. P. A. Mastorocostas and J. B. Theocharis. A dynamic fuzzy neural filter for separation of discontinuous adventitious sounds from vesicular sounds. *Comput Biol Med*, 37(1):60–69, Jan 2007.

42. P. A. Mastorocostas, Y. A. Tolias, J. B. Theocharis, L. J. Hadjileontiadis, and S. M. Panas. An orthogonal least squares-based fuzzy filter for real-time analysis of lung sounds. *IEEE Trans Biomed Eng*, 47(9):1165–1176, Sep 2000.

43. MathWorks. *MATLAB Signal Processing Toolbox User Guide.* MathWorks Inc, 2006.

44. D. Montgomery and G. Runger. *Applied Statistics and Probability for Engineers.* Wiley, 4 edition, 2006.

45. M. Munakata, H. Ukita, I. Doi, Y. Ohtsuka, Y. Masaki, Y. Homma, and Y. Kawakami. Spectral and waveform characteristics of fine and coarse crackles. *Thorax*, 46(9):651–657, Sep 1991.

46. R. L. Murphy, E. A. D. Bono, and F. Davidson. Validation of an automatic crackle (rale) counter. *Am Rev Respir Dis*, 140(4):1017–1020, Oct 1989.

47. R. L. Murphy, S. K. Holford, and W. C. Knowler. Visual lung-sound characterization by time-expanded wave-form analysis. *N Engl J Med*, 296(17):968–971, Apr 1977.

48. R. L. Murphy and K. Sorensen. Chest auscultation in the diagnosis of pulmonary asbestosis. *J Occup Med*, 15(3):272–276, Mar 1973.

49. A. Nath and L. Capel. Inspiratory crackles: early and late. *Thorax*, 29:223–227, 1974.

50. M. Ono, K. Arakawa, M. Mori, T. Sugimoto, and H. Harashima. Separation of fine crackles from vesicular sounds by a nonlinear digital filter. *IEEE Trans Biomed Eng*, 36(2):286–291, Feb 1989.

51. H. Pasterkamp, S. S. Kraman, and G. R. Wodicka. Respiratory sounds. advances beyond the stethoscope. *Am J Respir Crit Care Med*, 156(3 Pt 1):974–987, Sep 1997.

52. L. Pesu, P. Helistö, E. Ademovic, J. C. Pesquet, A. Saarinen, and A. R. Sovijärvi. Classification of respiratory sounds based on wavelet packet decomposition and learning vector quantization. *Technol Health Care*, 6(1):65–74, Jun 1998.

53. P. Piirilä, H. Lehtola, A. Zitting, L. Kivisaari, H. Koskinen, R. Luukkonen, S. P. Salo, T. Vehmas, H. Nordman, and A. R. Sovijärvi. Lung sounds in asbestos induced pulmonary disorders. *Eur Respir J*, 16(5):901–908, Nov 2000.

54. P. Piirilä and A. R. Sovijärvi. Crackles: recording, analysis and clinical significance. *Eur Respir J*, 8(12):2139–2148, Dec 1995.

55. P. Piirilä, A. R. Sovijärvi, T. Kaisla, H. M. Rajala, and T. Katila. Crackles in patients with fibrosing alveolitis, bronchiectasis, copd, and heart failure. *Chest*, 99(5):1076–1083, May 1991.

56. P. Piirila, K. Kallio, and T. Katila. Crackle sound intensity in the auscultation of crackling sounds in fibrosing alveolitis and heart failure. In *17th Int Conf on Lung Sounds*, volume 8, pages 24–26, 1992.

57. B. Sankur, E. C. Güler, and Y. P. Kahya. Multiresolution biological transient extraction applied to respiratory crackles. *Comput Biol Med*, 26(1):25–39, Jan 1996.

58. B. Sankur, Y. P. Kahya, E. C. Guler, and T. Engin. Comparison of ar-based algorithms for respiratory sounds classification. *Comput Biol Med*, 24(1):67–76, Jan 1994.

59. H. J. Schreur, J. Vanderschoot, A. H. Zwinderman, J. H. Dijkman, and P. J. Sterk. Abnormal lung sounds in patients with asthma during episodes with normal lung function. *Chest*, 106(1):91–99, Jul 1994.

60. G. Schwarz. Estimating the dimension of a model. *Ann Statistics*, 6(2):461–464, 1978.

61. R. Seeley, T. Stephens, and P. Tate. *Essentials of Anatomy and Physiology*. McGraw-Hill, 2 edition, 1996.

62. I. Sen. multi-channel device for respiratory sound data acquisition and transient detection. Master's thesis, Bogazici University, Dept. of Electrical and Electronic Eng., 2005.

63. I. Sen and Y. Kahya. A multi-channel device for respiratory sound data acquisition and transient detection. *Conf Proc IEEE Eng Med Biol Soc*, 6:6658–6661, 2005.

64. A. Sovijärvi, F. Dalmasso, J. Vanderschoot, L. Malmberg, G. Righini, and S. Stoneman. Definition of terms for applications of respiratory sounds. *Eur Respir Rev*, 77:597–610, 2000.

65. A. Sovijärvi, L. Malmberg, G. Charbonneau, J. Vanderschoot, F. Dalmasso, C. Sacco, M. Rossi, and J. Earis. Characteristics of breath sounds and adventitious respiratory sounds. *Eur Respir Rev*, 77:591–596, 2000.

66. A. R. Sovijärvi, P. Piirilä, and R. Luukkonen. Separation of pulmonary disorders with two-dimensional discriminant analysis of crackles. *Clin Physiol*, 16(2):171–181, Mar 1996.

67. G. Tortora and S. Grabowski. *Introduction to the Human Body: the Essentials of Anatomy and Physiology*. Wiley: New York, 6 edition, 2004.

68. L. Vannuccini, J. Earis, and P. Helistö. Capturing and preprocessing of respiratory sound. *Eur Respir Rev*, 77:616–620, 2000.

69. A. Vyshedskiy, F. Bezares, R. Paciej, M. Ebril, J. Shane, and R. Murphy. Transmission of crackles in patients with interstitial pulmonary fibrosis, congestive heart failure, and pneumonia. *Chest*, 128(3):1468–1474, Sep 2005.

70. G. R. Wodicka, K. N. Stevens, H. L. Golub, E. G. Cravalho, and D. C. Shannon. A model of acoustic transmission in the respiratory system. *IEEE Trans Biomed Eng*, 36(9):925–934, Sep 1989.

71. R. Xu and D. W. II. Survey of clustering algorithms. *IEEE Trans on Neural Networks*, 16:645–678, 2005.

72. N. Yasuda, K. Gotoh, Y. Yagi, K. Nagashima, T. Sawa, M. Nomura, S. Hirakawa, and H. Fujiwara. Mechanism of posturally induced crackles as predictor of latent congestive heart failure. *Respiration*, 64(5):336–341, 1997.

73. M. Yeginer and Y. Kahya. Modeling of pulmonary crackles using wavelet networks. *Conf Proc IEEE Eng Med Biol Soc*, 7:7560–7563, 2005.

74. M. Yeginer and Y. P. Kahya. Elimination of vesicular sounds from pulmonary crackle waveforms. *Comput Methods Programs Biomed*, 89(1):1–13, Jan 2008.

75. Q. Zhang and A. Benveniste. Wavelet networks. *IEEE Trans Neural Netw*, 3(6):889–898, 1992.

76. X. S. Zhang, Y. S. Zhu, N. V. Thakor, Z. M. Wang, and Z. Z. Wang. Modeling the relationship between concurrent epicardial action potentials and bipolar electrograms. *IEEE Trans Biomed Eng*, 46(4):365–376, Apr 1999.

77. E. Zwicker and H. Fastl. *Psychoacoustics*. Springer, 2 edition, 1999.